A Review of Planetary Boundary Layer Parameterization Schemes and Their Sensitivity in Simulating Southeastern U.S. Cold Season Severe Weather Environments

ARIEL E. COHEN

NOAA/NWS/NCEP/Storm Prediction Center, and School of Meteorology, University of Oklahoma, Norman, Oklahoma

STEVEN M. CAVALLO

School of Meteorology, University of Oklahoma, Norman, Oklahoma

MICHAEL C. CONIGLIO AND HAROLD E. BROOKS

NOAA/National Severe Storms Laboratory, Norman, Oklahoma

(Manuscript received 4 September 2014, in final form 2 January 2015)

ABSTRACT

The representation of turbulent mixing within the lower troposphere is needed to accurately portray the vertical thermodynamic and kinematic profiles of the atmosphere in mesoscale model forecasts. For mesoscale models, turbulence is mostly a subgrid-scale process, but its presence in the planetary boundary layer (PBL) can directly modulate a simulation's depiction of mass fields relevant for forecast problems. The primary goal of this work is to review the various parameterization schemes that the Weather Research and Forecasting Model employs in its depiction of turbulent mixing (PBL schemes) in general, and is followed by an application to a severe weather environment. Each scheme represents mixing on a local and/or nonlocal basis. Local schemes only consider immediately adjacent vertical levels in the model, whereas nonlocal schemes can consider a deeper layer covering multiple levels in representing the effects of vertical mixing through the PBL. As an application, a pair of cold season severe weather events that occurred in the southeastern United States are examined. Such cases highlight the ambiguities of classically defined PBL schemes in a cold season severe weather environment, though characteristics of the PBL schemes are apparent in this case. Low-level lapse rates and storm-relative helicity are typically steeper and slightly smaller for nonlocal than local schemes, respectively. Nonlocal mixing is necessary to more accurately forecast the lower-tropospheric lapse rates within the warm sector of these events. While all schemes yield overestimations of mixed-layer convective available potential energy (MLCAPE), nonlocal schemes more strongly overestimate MLCAPE than do local schemes.

1. Introduction

One substantial source of forecast inaccuracy in mesoscale models[1] is the representation of lower-tropospheric thermodynamic and kinematic structures (Jankov et al. 2005; Stensrud 2007; Hacker 2010; Hu et al. 2010; Nielsen-Gammon et al. 2010). The accurate representation of these structures is critical in improving forecasts of high-impact weather phenomena for which model output can aid in the assessment of whether necessary conditions for such phenomena would be met (e.g., Kain et al. 2003, 2005, 2013). As an example, for organized severe thunderstorms [those producing wind gusts of at least 26 m s^{-1}, tornadoes, and/or hail of at least 25.4 mm (1 in.) in diameter], the necessary conditions are moisture, lift, instability, and vertical wind shear, which are highly variable across the wide spectrum of convection that ensues (e.g., Johns and Doswell 1992; Rasmussen and Blanchard 1998; Thompson et al. 2003; Craven and Brooks 2004; Schneider and Dean 2008). A simulation of the particular intricacies of such

[1] Herein, we refer to models with grid spacing fine enough to allow explicit representation of convection (~1–4 km) as mesoscale models because the smallest fully resolvable scales are typically in the meso-γ-scale range.

Corresponding author address: Ariel Cohen, Storm Prediction Center, 120 David L. Boren Blvd., Norman, OK 73072.
E-mail: ariel.cohen@noaa.gov

DOI: 10.1175/WAF-D-14-00105.1

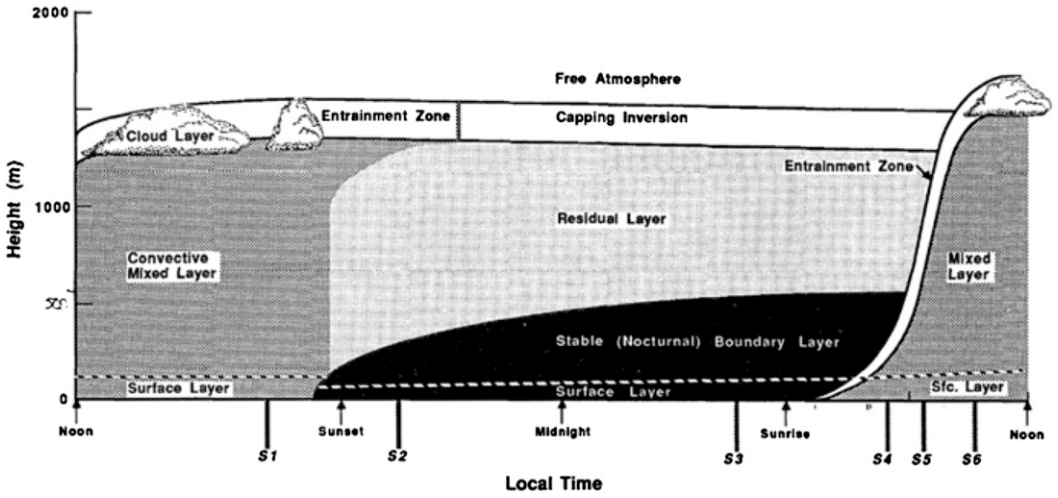

FIG. 1. Constituents of the PBL and their evolution through the diurnal and nocturnal cycles [from Kis and Straka (2010) and Stull (1988)].

an environment is heavily influenced by its depiction of the planetary boundary layer (PBL)—that portion of the lower troposphere directly affected by the earth's surface via troposphere–surface exchanges of heat, moisture, and momentum on subhourly time scales (e.g., Stull 1988; Stensrud 2007).

Exchanges of moisture, heat, and momentum occur within the PBL through mixing associated with turbulent eddies. These eddies influence the way in which lower-tropospheric thermodynamic and kinematic structures evolve. Such eddies operate on spatiotemporal scales that cannot be explicitly represented on grid scales and time steps employed in most mesoscale models. As such, their effects are expressed in these models via the use of PBL parameterization schemes, whose theoretical development is outlined in multiple sources addressing the subject (e.g., Stull 1988; Holton 2004; Stensrud 2007).

This paper reviews the processes for which mesoscale models represent the evolution of turbulent motions within the lower troposphere. Characteristics of several PBL schemes within the Advanced Research version of the Weather Research and Forecasting (WRF) Model (ARW; Skamarock et al. 2008) are summarized, first in the general sense for a variety of environmental stability conditions. This summary is synthesized through the larger body of contemporary PBL-related research. As an example of an application of the aforementioned synthesis, we examine PBL-scheme sensitivity for a situation that is notably challenging for the forecasting of severe convective storms: the southeastern U.S. cold season severe thunderstorm environment.

During cold season tornado events in the southeastern United States, Guyer et al. (2006) and Guyer and Dean (2010) note that buoyancy tends to be limited and vertical wind shear tends to be large in the near-storm environment. Ashley (2007) concludes that this part of the country is particularly vulnerable to tornado fatalities owing to the mutual overlap of favorable climatological, land-use, and societal patterns, which highlights the need for improving forecast accuracy of these events. In a study of tornadoes rated as category 2 or higher on the Fujita scale (F2) that occurred across the southeastern United States during the cold season from 15 October to 15 February 1984–2004, Guyer et al. (2006) highlight modest moisture and instability as the primary mitigating factors for organized severe convection amid a background synoptic environment more commonly supporting strong vertical wind shear. However, in some circumstances, sufficient, albeit limited, CAPE does develop for deep convection with significant tornadoes, and they conjecture that this CAPE originates from the relatively warm and moist low levels within the warm sector of an extratropical cyclone.

The prediction of severe thunderstorms can be particularly challenging for environments in which one or more of the necessary conditions are marginally supportive of severe weather, in which small errors can be very meaningful (e.g., Vescio and Thompson 1998). This may be a reason why southeastern U.S. cold season severe weather has not been extensively studied, especially in regard to mesoscale modeling and related PBL schemes. Factors like shear-driven eddies and large-scale vertical motion influence the thermodynamic and

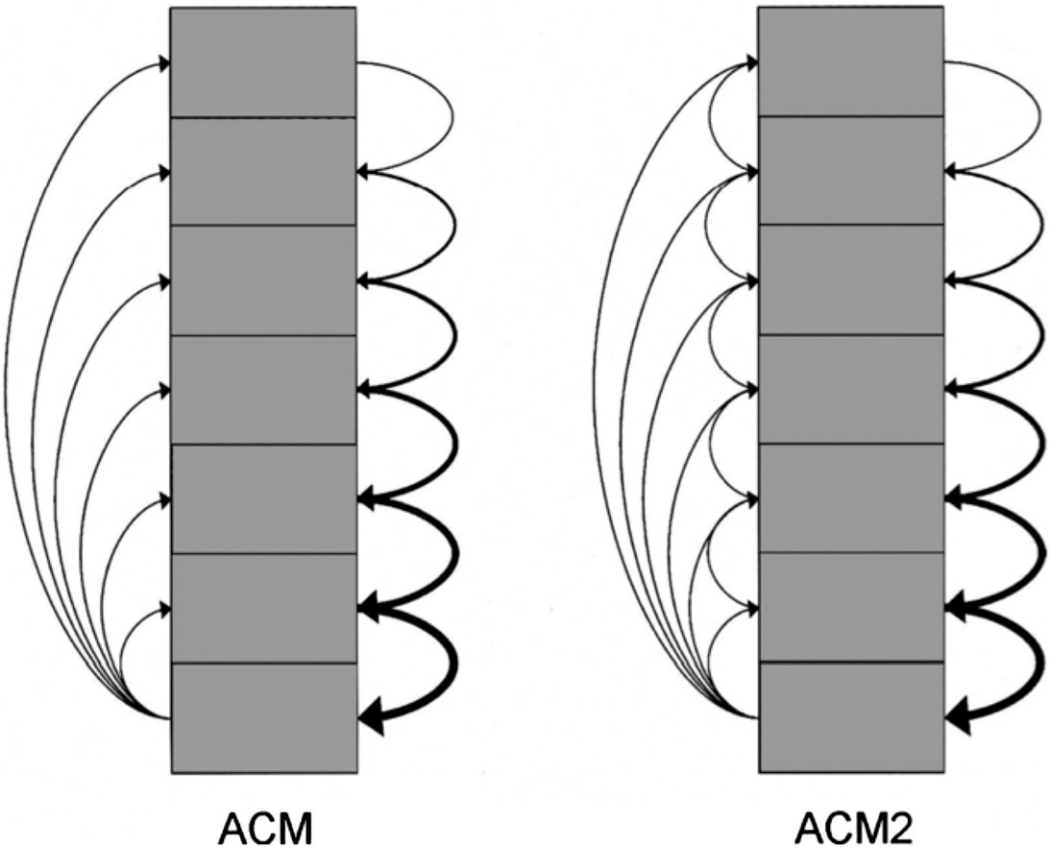

FIG. 2. Depiction of the mechanics of the ACM and ACM2 schemes regarding PBL interactions [from Pleim (2007a)]. Arrows depict exchanges of atmospheric quantities between various layers within the simulated PBL.

kinematic properties of the PBL in this regime, in addition to heat fluxes from diurnal heating. In fact, through field observations and computer visualizations, Schneider and Lilly (1999) specifically identify vertical wind shear as a contributor to the production of turbulence, which influences the makeup of the PBL, and it is uncertain how these complicating effects are manifest in the accuracy of PBL schemes. Thus, examining the characteristics among the PBL schemes for the southeastern U.S. cold season severe weather environment is a step toward identifying their potential weaknesses that may lead to forecast bias.

2. Theoretic foundation of PBL parameterization schemes

Among other texts, Stensrud (2007) and Stull (1988) provide explanations of the process by which turbulence is mathematically represented in numerical weather prediction models. There are two major components of this process: the order of turbulence closure and whether a local or nonlocal mixing approach is employed.

a. Order of turbulence closure

The theoretical development of PBL parameterization schemes requires the decomposition of variables of the equations of motion into mean and perturbation components. The mean components represent the time-averaged conditions that characterize the background atmospheric state. The perturbation components represent deviations, or turbulent fluctuations, from the background mean state, which are inherent to turbulent motions (i.e., what the perturbations describe) within the PBL. Equations pertaining to turbulence modeling will always contain more unknown terms than known terms, where the unknown term is always of one order above the maximum among the other terms. Because of this, turbulence closure requires empirically relating the unknown term of moment $n + 1$ to lower-moment known terms. This is referred to as nth-order turbulence closure, where n is an integer. Some PBL schemes are considered noninteger orders. For example, 1.5-order closure parameterization schemes predict second-order turbulent kinetic energy (TKE) by diagnosing second-order moments for some variables (i.e., variances of potential temperature and mixing ratio and their related

TABLE 1. Listing of WRF PBL schemes, along with a reference, a brief description, and selected advantages and disadvantages. Different text styles represent classes of PBL scheme type (i.e., nonlocal in exclusively boldface, local in exclusively italics, and hybrid local–nonlocal in boldface and italics).

PBL scheme name, type, and reference	Description	Advantage(s)	Disadvantage(s)
MRF, nonlocal, Hong and Pan (1996)	**First-order closure; follows Troen and Mahrt (1986) concept of incorporating a countergradient correction term into downgradient diffusion expressed solely by local mixing**	**Compared to local PBL schemes, MRF more accurately simulates the deeper mixing within an unstable PBL where larger eddies entrain higher potential temperatures above the PBL into the PBL (e.g., Stull 1993; Wyngaard and Brost 1984)**	**Depicts too deep of a PBL, especially in strong-wind regimes at night (Mass et al. 2002); too deep of mixing results in overerosion of convective initiation (Bright and Mullen 2002)**
YSU, nonlocal, Hong et al. (2006)	**First-order closure; similar to MRF, except YSU represents entrainment at the top of the PBL explicitly**	**More accurately simulates deeper vertical mixing in buoyancy-driven PBLs with shallower mixing in strong-wind regimes compared to MRF (Hong et al. 2006)**	**Has still been found to overdeepen the PBL for springtime deep convective environments, resulting in too much dry air near the surface and underestimation of MLCAPE related to environments of deep convection (Coniglio et al. 2013)**
MYJ, local, Janjić (1990, 1994)	*A 1.5-order closure scheme with an equation for prognosis of TKE*	*Improves upon Mellor–Yamada 1.5-order local scheme (Mellor and Yamada 1974, 1982) without particularly large computational expense*	*Undermixes PBL for locations upstream of spring convection (e.g., Coniglio et al. 2013)*
QNSE, local, Sukoriansky et al. (2005)	*Similar to MYJ, QNSE invokes 1.5-order local closure and is intended to account for wave phenomena within stable boundary layers*	*Provides realistic depiction of potential temperature profiles, PBL height, and kinematic profiles based on observational data and corresponding large eddy simulations (Kosović and Curry 2000) for its designed environment (stable conditions)*	*As with the MYJ scheme, in the case of the less-stable PBL, QNSE depicts too cool, moist, and shallow of a PBL for simulations of springtime convective environments*
MYNN, local, Nakanishi and Niino (2004, 2006)	*Both 1.5- (MYNN2) and second-order (MYNN3) closure schemes; compared to the Mellor–Yamada PBL scheme (Mellor and Yamada 1974, 1982), expressions of stability and mixing length are based on the results of large eddy simulations rather than on observations, while the expressions of mixing length are more applicable to a variety of static stability regimes*	*MYNN2 involves less computational expense than MYNN3; MYNN3 more accurately portrays deeper mixed layers compared to the Mellor–Yamada PBL scheme (Mellor and Yamada 1974, 1982); MYNN3 reasonably depicts statically stable boundary layer simulations supporting radiation fog development (Nakanishi and Niino 2006); MYNN2 improves the PBL depiction over nonlocal PBL schemes for springtime PBLs that support deep convection (Coniglio et al. 2013)*	*As with the MYJ, the local formulations of the MYNN2 and MYNN3 still may not fully account for deeper vertical mixing associated with larger eddies and associated countergradient flux correction terms*
BouLac, local, Bougeault and Lacarrère (1989)	*A 1.5-order local closure including a prognostic equation for TKE; design is relevant for terrain-enhanced turbulence (e.g., wave phenomena) and its impact on the PBL*	*Found to better represent the PBL in regimes of higher static stability compared to nonlocal schemes in similar regimes (Shin and Hong 2011)*	*As with the MYNN entry above*

TABLE 1. (*Continued*)

PBL scheme name, type, and reference	Description	Advantage(s)	Disadvantage(s)
Grenier–Bretherton–McCaa (GBM), local, Grenier and Bretherton (2001)	*A 1.5-order local closure to depict a PBL influenced by stratocumulus clouds; vertical variations in static stability profiles are driven by longwave radiation fluxes owing to the presence of these clouds; vertical fluxes of TKE are enhanced for better comparison to large eddy simulations*	*Reductions to the stratocumulus cloud deck owing to vertical mixing are found to be well handled for vertical grid spacing at or smaller than 15 mb; this could be relevant for depicting the impact of stratocumulus clouds on buoyancy preceding potentially severe convection*	*As with the MYNN and BouLac entries above*
University of Washington moist turbulence (UWMT), local, Bretherton and Park (2009)	*A 1.5-order local closure; attempts to improve upon the GBM; changes from the GBM include accounting for relatively longer time steps relevant for climate models, diagnosing rather than forecasting TKE, and focusing computations over a number of layers determined by the vertically varying stability of the thermodynamic profile*	*Provides more accurate depiction of a nighttime stable boundary layer; substratocumulus layers that are too moist relative to results from large eddy simulations based on the Holtslag and Boville (1993) nonlocal PBL scheme are less moist and well mixed using the UW scheme*	*As with the MYNN, BouLac, and GBM entries above*
ACM2, hybrid local–nonlocal, Pleim (2007a)	***First-order closure; representation of upward fluxes within the PBL as interactions between the surface layer and each and every layer above (with local eddy diffusion also included), while downward fluxes extend from each layer to each immediately underlying layer (Fig. 2); this represents convective plumes arising from the diurnally heated surface layer, whereas downward fluxes are more gradual***	***Pleim (2007a) indicates that the profile of potential temperature and velocity through the PBL are depicted with greater accuracy when both local and nonlocal viewpoints are considered regarding vertical mixing (ACM2); Pleim (2007b) further validates the use of the ACM2 scheme owing to its support of PBL heights similar to those based on afternoon wind profiler data from radar***	***Coniglio et al. (2013) reveal evening soundings supporting deep convection with too-deep PBLs represented by the ACM2 scheme***
TEMF, hybrid local–nonlocal, Angevine et al. (2010)	***A 1.5-order closure; nonlocal component represented by updrafts owing to upward heat fluxes from the surface that provide mass fluxes through the PBL (countergradient correction) (Angevine 2005); local component activated under statically stable conditions using the total turbulent energy concept that eliminates buoyant destruction of TKE in high static stability (Mauritsen et al. 2007)***	***Compares favorably with large eddy simulation results for observations from the 2006 Texas Air Quality and Gulf of Mexico Atmospheric Composition and Climate Study (TexAQS II/GoMACCS) around Houston, Texas (Angevine et al. 2010); yields PBL profiles more accurately depicting scenarios supporting shallow cumulus clouds than other schemes (Angevine et al. 2010)***	***Indicates greater drying beneath stratocumulus clouds and higher moisture content within the lower cloud layer compared to results from the large eddy simulations, indicating too much moisture flux across the lower cloud boundary in the TEMF scheme (Angevine et al. 2010)***

covariances) (e.g., Stensrud 2007; Coniglio et al. 2013) and first-order moments for other variables. TKE quantifies the perturbation component of motion, characterizing the magnitude of turbulence in the PBL owing to vertical wind shear, buoyancy, turbulent transport, and dampening driven by molecular viscosity (e.g., Holton 2004).

b. Local versus nonlocal PBL parameterization schemes

One important way that PBL schemes differ is according to the depth over which these known variables are allowed to affect a given point, determined on the sole basis of the vertical gradient of the perturbation quantities at the point and not horizontal gradients (e.g., Ching et al. 2014). In the case of local closure schemes, only those vertical levels that are directly adjacent to a given point directly affect variables at the given point. On the other hand, multiple vertical levels (e.g., those within the PBL) can be used to determine variables at a given point in nonlocal closure schemes. It is well understood that local schemes can offer a substantial disadvantage regarding their depiction of the PBL because

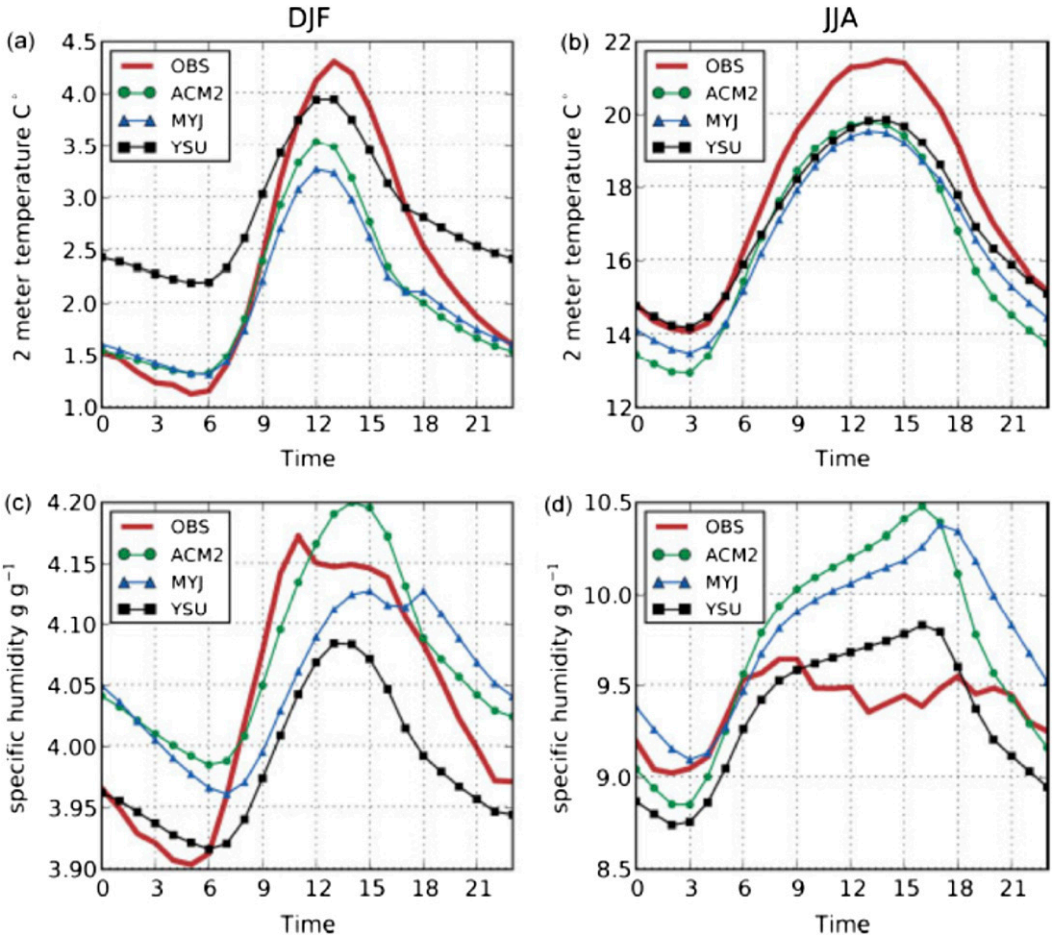

FIG. 3. Comparisons of WRF PBL schemes with European synoptic observations for temperatures during the (a) winter and (b) summer and for specific humidity during the (c) winter and (d) summer [from García-Díez et al. (2013)].

localized stability maxima through the vertical thermal profile are not necessarily representative of the overall state of mixing in the PBL (Stensrud 2007). Vertical mixing throughout the depth of the PBL is primarily accomplished by the largest eddies, which are often only minimally affected by local variations in static stability.

In local schemes, the PBL grows minimally in the presence of localized static stability maxima, in which the fluxes are downward from higher potential temperature to lower potential temperature. This is especially the case at the top of the simulated daytime PBL owing to higher static stability within the entrainment zone beneath the free atmosphere (Fig. 1). In the observed atmosphere, large eddies can transport heat upward from the diurnally heated surface layer regardless of the localized stability maxima and produce what are called countergradient fluxes (i.e., counter to the downward direction of heat fluxes accompanying stability maxima) (Stull 1988). These large eddies can penetrate the top of the mixed layer and entrain properties of the free atmosphere well into the mixed layer, thereby bolstering PBL depth. Nonlocal schemes account for these countergradient fluxes and, thus, generally represent deep PBL circulations more accurately than local schemes (Stull 1991). However, in some circumstances, the utility of local schemes can improve by invoking higher orders of closure (e.g., Mellor and Yamada 1982; Nakanishi and Niino 2009; Coniglio et al. 2013), though usually at a higher computational cost. Some schemes simultaneously represent both nonlocal and local mixing concepts [e.g., Asymmetric Convective Model, versions 1 and 2 (ACM and ACM2, respectively) in Fig. 2].

3. PBL schemes in the Weather Research and Forecasting Model

Operational forecasting needs have increasingly placed emphasis on using the output of high-resolution numerical models to simulate meso- and storm-scale processes accurately (e.g., Weiss et al. 2008). The

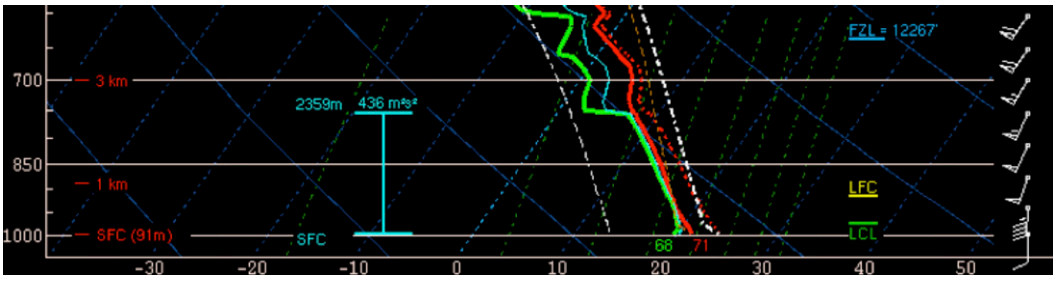

FIG. 4. The observed sounding at 0400 UTC 1 Jan 2011 in Jackson. Solid red trace indicates the environmental temperatures, dashed red trace indicates the environmental temperatures incorporating the virtual temperature correction, solid green trace indicates environmental dewpoint values, dashed thick white trace indicates the temperatures of an ascending surface-based parcel that incorporates the virtual temperature correction, dashed brown trace indicates the temperatures of an ascending surface-based parcel without incorporating the virtual temperature correction, dashed thin white trace indicates the temperatures for a descending parcel, light-blue trace between environmental temperature and dewpoint indicates wet-bulb temperatures, and vertical light-blue bracket indicates the effective-inflow layer (Thompson et al. 2007).

parameterization of the PBL by these models directly influences the models' portrayal of buoyancy and vertical wind shear, as well as precipitation evolution (e.g., Hong et al. 2006). Here, we investigate how the PBL evolves within the ARW, version 3.3.1, using 4-km grid spacing (e.g., Skamarock et al. 2008). Several studies have compared the performance of WRF PBL schemes in influencing the depicted PBL state, highlighting the sensitivity of the PBL state to the selected PBL scheme, and some of their more salient findings are summarized here for the benefit of the weather and forecasting community. These studies do not focus on the southeastern U.S. cold season severe thunderstorm environment, which will be a focus in subsequent sections. As a supplement, Table 1 defines the acronyms for the schemes used in WRF and provides a detailed overview of the schemes.

Xie et al. (2012) compare local and nonlocal schemes for simulations over Hong Kong and find that nonlocal-influenced schemes [i.e., ACM2 and Yonsei University (YSU)] yield deeper and more accurate PBLs than those depicted by local schemes [i.e., Mellor–Yamada–Janjić (MYJ) and Bougeault–Lacarrère (BouLac)]. These are related to differences in parameters relevant to severe storm forecasting, such as buoyancy via surface-layer modulations to potential temperature and mixing ratio associated with variability in the depth of stronger mixing. Likewise, Hu et al. (2010) find that, over the south-central United States in summer, the nonlocal YSU scheme and hybrid local–nonlocal ACM2 scheme yield the smallest biases in temperature and moisture in the lower atmosphere owing to diurnal mixing. YSU and ACM2 are generally characterized by warmer and drier daytime PBLs, which are more consistent with observations, while the MYJ scheme's purely local treatment of larger-scale eddies prevents the PBL from mixing as deeply to produce cooler and moister conditions. Similarly, Gibbs et al. (2011) find that the nonlocal YSU scheme and the hybrid local–nonlocal ACM2 scheme produces a drier PBL in a dry convective boundary layer (CBL) than the local MYJ scheme, with YSU and ACM2 better depicting the observed PBL than MYJ.

Regarding marine boundary layers, Huang et al. (2013) compare the total energy–mass flux (TEMF), YSU, MYJ, Mellor–Yamada–Nakanishi–Niino (MYNN), and Medium-Range Forecast Model (MRF) schemes to observations collected from three field experiments; MYNN, and especially TEMF, provide the least-biased thermodynamic structures. Huang et al. (2013) conclude that the inclusion of both local and nonlocal processes in TEMF results in more accurate PBL depictions in regimes for which stratocumulus and shallow cumulus clouds are present.

Ching et al. (2014) describe the inability for high-resolution models to reliably simulate convectively induced secondary circulations (CISCs; e.g., convective rolls) owing to the disparity between the smaller spatial scale related to the CISCs and the model's larger grid length. Model-simulated CISCs can arise as numerical artifacts, which have similar characteristics to those that naturally occur. However, these are in violation of the assumption that only vertical gradients in perturbation, turbulent quantities are considered by PBL schemes, as previously addressed. Ching et al. (2014) advocate the use of nonlocal PBL parameterization schemes to enhance the model's simulation of heat extraction from the surface while still representing fluxes associated with the secondary circulations. Without the representation of these processes, local PBL parameterization schemes reproduce the artifact, model CISCs, most prominently

using the local MYJ and quasi-normal scale elimination (QNSE) schemes across southeastern Louisiana and southeastern Mississippi.

4. The PBL in relation to southeastern U.S. cold season severe weather environments

A goal of this study is to address the lack of analyses of PBL-scheme sensitivity in environments that support severe weather in the southeastern United States during the cool season. However, there have been studies that examine PBL-scheme behavior in European warm season environments (e.g., García-Díez et al. 2013). These studies are relevant to the present work because there are many similarities between southeastern U.S. cold season severe weather environments and European (primarily warm season) severe storm environments. Brooks (2009) shows that CAPE and deep-layer shear combinations associated with significantly severe thunderstorms in Europe are more similar to those associated with the southeastern U.S. cold season than the entire full-U.S. distribution. These environments are exhibited by limited buoyancy along with low-altitude lifting condensation levels (LCLs). Strong large-scale forcing for ascent provides the backdrop for European severe storm environments to offset the limited buoyancy, as is often the case with southeastern U.S. cold season severe storm environments (Brooks 2009). Therefore, comparisons between PBL scheme performance during European warm and cold seasons could provide direction for anticipating the effects of choosing a given PBL scheme representing southeastern U.S. cold season severe thunderstorm environments.

García-Díez et al. (2013) highlight the diurnal, seasonal, and geographical sensitivities of PBL schemes over Europe (Fig. 3), and show cold biases in surface temperatures throughout the summer. The MYJ scheme results in the most substantial cold biases during the daytime, compared to the YSU and ACM2 schemes, with the YSU scheme most commonly exhibiting the warmest temperatures among the three schemes throughout the day and night. This relatively low bias in using YSU is attributed to its ability to more accurately account for the stronger entrainment processes within the PBL, consistent with our expectation that YSU's nonlocal treatment of PBL processes should promote a relatively deeper PBL. Furthermore, YSU is found to yield a significantly deeper PBL during the daytime. When compared to gridded precipitation and 2-m temperature observations over Europe, Haylock et al. (2008) further substantiate the findings of García-Díez et al. (2013) and conclude that the warm season cold bias is relatively lower when using the YSU scheme.

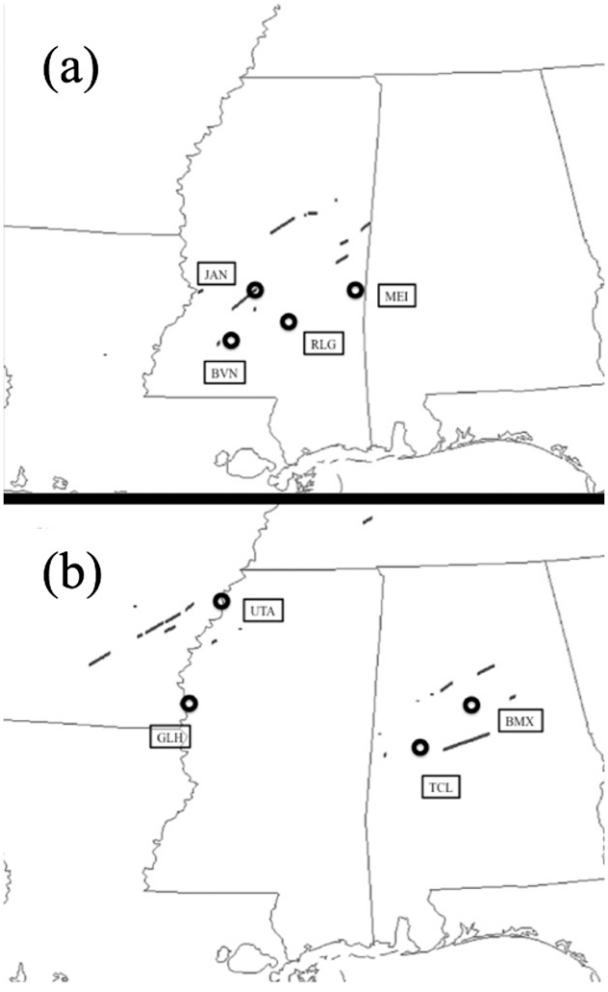

FIG. 5. Tornado paths marked as black segments from (a) 1200 UTC 31 Dec 2010 to 1200 UTC 1 Jan 2011 and (b) 1200 UTC 22 Jan to 1200 UTC 23 Jan 2012 (Storm Prediction Center 2013a). Black ovals indicate locations of sounding analyses in the present study, with city identifiers listed beside the ovals [Jackson (JAN), Brookhaven (BVN), Raleigh (RLG), Meridian (MEI), Greenville (GLH), Tunica (UTA), Tuscaloosa (TCL), and Birmingham (BMX)].

Therefore, we believe that the YSU scheme, which is a nonlocal scheme, could offer some utility in forecasts for southeastern U.S. cold season severe weather environments among the other PBL schemes currently available in the WRF Model. Furthermore, García-Díez et al. (2013) stress that long-term statistical studies have a tendency of masking important biases among PBL schemes owing to bias cancellation on smaller spatiotemporal scales. As such, they specifically encourage studies that support the advancement of PBL schemes in environments that have not been examined thoroughly (e.g., the southeastern U.S. cold season severe weather environment).

To illustrate a vertical profile for cold season severe weather events in the United States, we present the

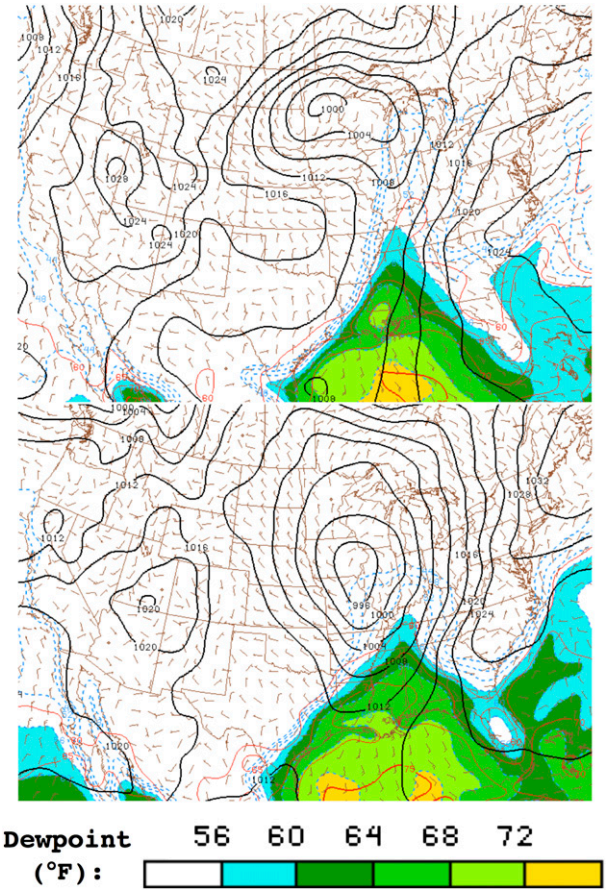

FIG. 6. Mesoanalysis output (Storm Prediction Center 2013b) based on surface objective analysis (Bothwell et al. 2002) at (top) 0400 UTC 1 Jan 2011 and (bottom) 0600 UTC 23 Jan 2012 for mean sea level pressure (mb; black contours with 4 mb interval), surface isotherms {°F; equivalent to [°C(1.8 + 32)]; red contours with 5°F interval}, surface isodrosotherms (°F; dashed contours with 4°F interval and color fill indicating dewpoint values ≥56°F), and surface winds [m s^{-1}; barbs with full wind barbs corresponding to 5 m s^{-1} (10 kt) and half barbs to 2.5 m s^{-1}].

sounding provided by a special radiosonde that was launched at 0400 UTC 1 January 2011 in Jackson, Mississippi (Fig. 4), within relatively close spatiotemporal proximity (within 100 km and 3 h) to some of the central Mississippi tornadoes, with simulations of this event later addressed in this paper. This sounding appears to be representative of the inflow to related storms and highlights some of the complexities regarding the characterization of the PBL structure for this particular environment. A shallow layer, extending from the surface to around 0.5 km above the ground, features relatively steep lapse rates within a deeper layer of small temperature–dewpoint spread (i.e., moist layer) below ~750 mb in which potential temperature increases with height and mixing ratio also decreases with height, aside from the little variability in mixing ratio within the lowest 100 mb. Despite the lack of steeper lapse rates that would otherwise be associated with stronger mixing, moisture is sufficient in the low levels to support nonzero buoyancy. Surmounting the moist layer are multiple layers of lower static stability and vertical moisture gradients, representative of the free atmosphere illustrated in Fig. 1. The event corresponding to this profile is simulated with results addressed in subsequent sections.

TABLE 2. Makeup of the WRF ensemble testing sensitivity owing to PBL scheme choice.

PBL scheme	Compatible surface-layer scheme and corresponding reference
YSU	MM5 similarity Monin–Obukhov; Monin and Obukhov (1954)
QNSE	QNSE PBL surface layer; Sukoriansky et al. (2005)
MYJ	Eta similarity Monin–Obukhov (Janjić Eta); Janjić (1996)
ACM2	MM5 similarity Monin–Obukhov; Monin and Obukhov (1954)
MRF	MM5 similarity Monin–Obukhov; Monin and Obukhov (1954)

The vertical wind profile is not consistent with our expectations of a well-mixed PBL through the aforementioned moist layer (extending from the surface to around the 700-mb level in Fig. 4). This is attributed to jet-induced vertical wind shear associated with a large-scale extratropical cyclone. In terms of this southeastern U.S. cold season environment, the poorly mixed vertical wind profile is one in which both wind speed and direction vary with increasing height through the moist layer. In particular, relatively weak southerly flow near the surface veers to southwesterly flow with a speed around 26 m s^{-1} [50 knots (kt; 1 kt = 0.51 m s^{-1})] at 850 mb. The backed surface flow relative to that aloft and the increase in wind speeds with heights, perhaps bolstered by friction-induced weakening of the flow near the surface, supports large storm-relative helicity (SRH; e.g., Davies-Jones et al. 1990) of 375–425 m^2 s^{-2} within the 0–1- and 0–3-km layers.

The 1 January 2011 example highlights the complications in defining an upper bound of the PBL in a sample southeastern U.S. cold season severe storm environment. Vertical potential temperature, mixing ratio, and wind profiles are not well mixed throughout the lower troposphere, and there is no clear demarcation of any atmospheric variables that might characterize the "top" of the PBL. Using the cloud base, or the LCL for the purposes of this work, to define the PBL top (e.g., Stull 1988) may exclude the role that the poorly mixed vertical wind profile and accompanying shear-driven,

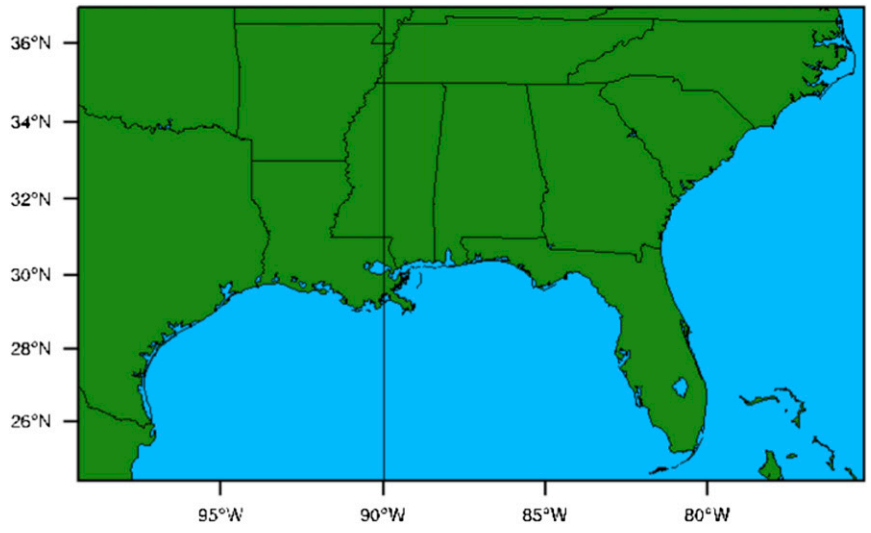

FIG. 7. WRF domain for the simulations.

mechanical production of turbulence offer in communicating surface forcing upward to define a PBL. Mechanically produced turbulence communicates surface conditions through the lower troposphere such that thermodynamic profiles may provide few clues regarding the bounds of the PBL, as they would otherwise do through a large part of the literature review previously discussed, complicating their utility in the southeastern U.S. cold season severe thunderstorm environment regime for defining the PBL.

5. PBL schemes for southeastern U.S. cold season severe weather environments

a. Evaluation methodology

In a somewhat analogous manner to WRF scheme comparisons for the European PBL, PBL-scheme behavior is examined for two southeastern U.S. tornado events that occurred in the lower Mississippi River valley and central Gulf Coast region: 1) from 31 December 2010 to 1 January 2011 and 2) from 22 to 23 January 2012 (tornado reports in Fig. 5). These case studies are presented here to illustrate the PBL scheme concepts that are potentially relevant to southeastern U.S. severe weather, and are part of an analysis of a much larger set of cases that is ongoing and will be presented in a future study. Most of the tornado reports corresponding to the first event occurred from 2200 UTC 31 December 2010 to 1000 UTC 1 January 2011, and most of the tornado reports corresponding to the second event occurred after 0100 UTC 23 January 2012. The surface pattern during both of these severe weather events promoted strong poleward heat and moisture transport inland of the Gulf of Mexico. In each case, a roughly wedge-shaped warm sector characterized by rich Gulf moisture extending inland well to the south-southeast of an extratropical cyclone centered over the upper Mississippi River valley (Fig. 6).

First, we investigate the sensitivity of five WRF PBL schemes in simulating severe convection–relevant parameters for these cases. This is accomplished by producing WRF forecasts with varying PBL schemes but otherwise identical experiment configurations, as shown in Table 2. Initial and boundary conditions are from the National Centers for Environmental Prediction Final (FNL) Operational Global Analysis (NCAR 2013). The simulations contain 50 vertical levels across a horizontal domain that extends from the northern Gulf of Mexico northward to areas extending from parts of Oklahoma to portions of Tennessee (Fig. 7). For all five WRF simulations, we use a horizontal grid spacing of 4 km, the WRF single-moment 6-class microphysics scheme (Hong and Lim 2006), the Rapid Radiative Transfer Model relevant for general circulation models (RRTMG; Iacono et al. 2008) long- and shortwave radiation schemes, the Noah land surface model (Ek et al. 2003), a model time step of 12 s, and a radiation time step of 30 min. The first simulation is initialized at 1200 UTC 31 December 2010 and ends at 1200 UTC 1 January 2011, and the second simulation is initialized at 1200 UTC 22 January and ends at 1200 UTC 23 January 2012. FNL-based boundary conditions are updated every 6 h.

PBL-scheme sensitivities are examined by focusing on a few parameters in the warm sector of the synoptic cyclone that forecasters commonly consider when predicting severe storms. As an example of the diversity of solutions that result by adjusting the PBL scheme,

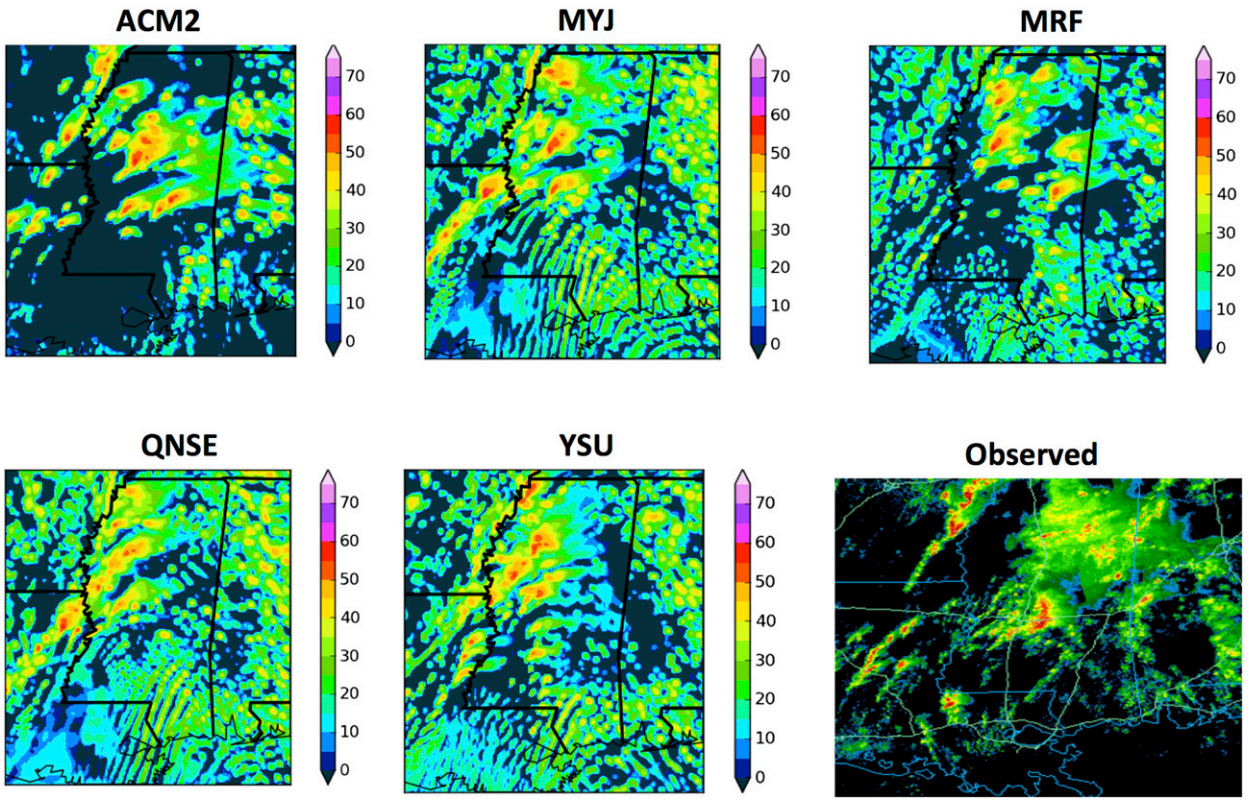

FIG. 8. The 12-h forecast of simulated composite reflectivity (dBZ) for each WRF PBL member valid at 0000 UTC 1 Jan 2011 and the observed mosaic composite reflectivity [from University Corporation for Atmospheric Research (2014)] at 2357 UTC 31 Dec 2010.

simulated environmental differences among the various PBL schemes are manifest in different simulated reflectivity patterns (Fig. 8). These differences can influence a forecaster's assessment of the severe weather potential. The tendency for nonlocal PBL parameterization schemes to suppress artificial CISCs (Ching et al. 2014) is well illustrated in Fig. 8: local PBL parameterization schemes produce artificial CISCs in this environment, especially the MYJ and QNSE schemes across southeastern Louisiana and southeastern Mississippi.

Aside from the special sounding at 0400 UTC 1 January 2011 shown earlier (Fig. 4), no in situ observational data regarding the near-storm environment of tornadic storms is available for these two cases. Direct observations of the near-storm thermodynamic and kinematic environments are restricted to the routine National Weather Service (NWS) radiosonde observations taken at 1200 or 0000 UTC, which did not represent the near-storm environments. As such, we combine Rapid Update Cycle (RUC) model output with objectively analyzed surface observations to reconstruct a proxy for the real environment, as is done for the Storm Prediction Center (SPC) surface objective analysis (SFCOA) fields [Bothwell et al. (2002); details are provided in the appendix]. Although the accuracy of the RUC–SFCOA fields in southeastern U.S. severe weather regimes is not well known, the SFCOA fields were found to be quite accurate for central U.S. severe weather regimes (Coniglio 2012).

Lower-tropospheric RUC profiles are inherently influenced by the 1.5-order PBL scheme from Burk and Thompson (1989). This PBL scheme is a local scheme, and it is uncertain to what extent, if any, this scheme potentially misdiagnoses PBL mixing and corresponding kinematic and thermodynamic profiles in the evaluation of the WRF simulations. Regardless, the inclusion of SFCOA fields, which are directly influenced by surface observations, is a key component of effectively adjusting the lower boundary of these profiles as close as is objectively possible to observational data, to enhance the viability of the RUC–SFCOA dataset in representing reality.

WRF output for each of the PBL schemes is compared with reconstructed RUC–SFCOA soundings at four locations in proximity to the tornadoes for each case (identified in Fig. 5). The comparison of the simulated storm environments to observations in this particular environment requires great care, because the warm-sector geometry and convective processes evolved very rapidly during this event. Such an evaluation is different

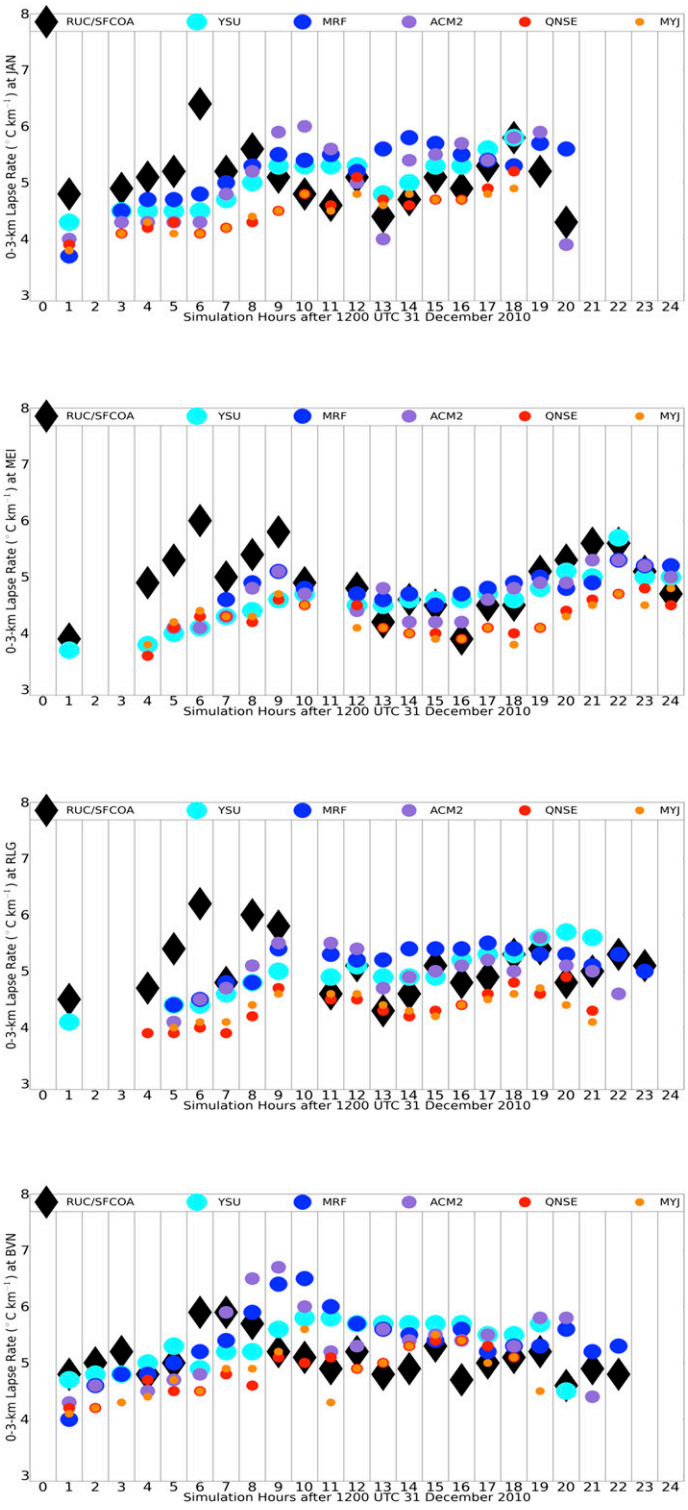

FIG. 9. Time series of 0–3-km lapse rates for WRF simulations (after 1200 UTC 31 Dec 2010) and RUC–SFCOA output at sites (from top to bottom) JAN, MEI, RLG, and BVN (as identified in Fig. 5). Color and shape of the markers denotes the PBL scheme used in the WRF simulation and RUC–SFCOA output, as indicated in the legends. Cool colors (shades of blue) refer to nonlocal schemes, warm colors (red and orange) to local schemes, purple to the hybrid scheme (e.g., ACM2), and black to RUC–SFCOA output. Missing data imply convectively contaminated soundings.

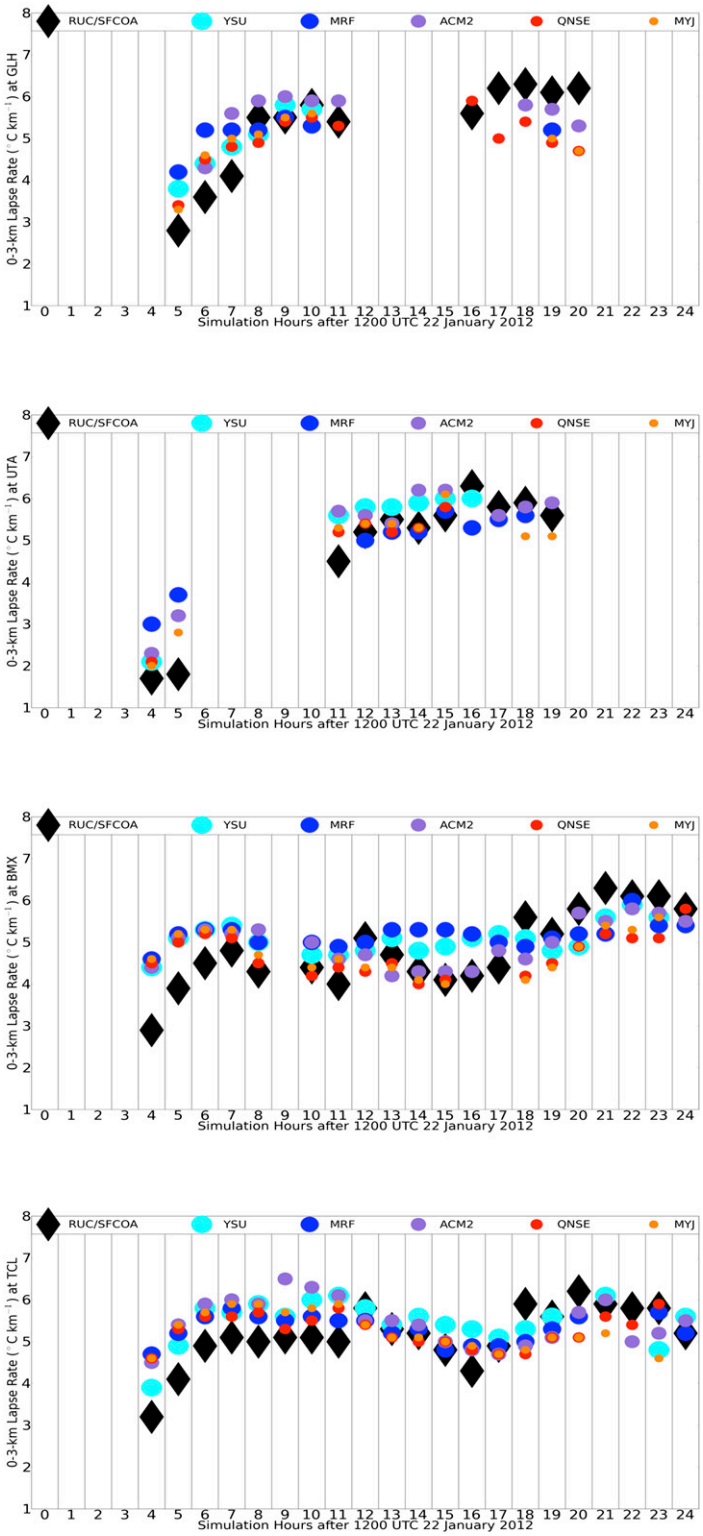

FIG. 10. As in Fig. 9, but for WRF simulations (after 1200 UTC 22 Jan 2012) and RUC–SFCOA output at sites (from top to bottom) GLH, UTA, BMX, and TCL (as identified in Fig. 5).

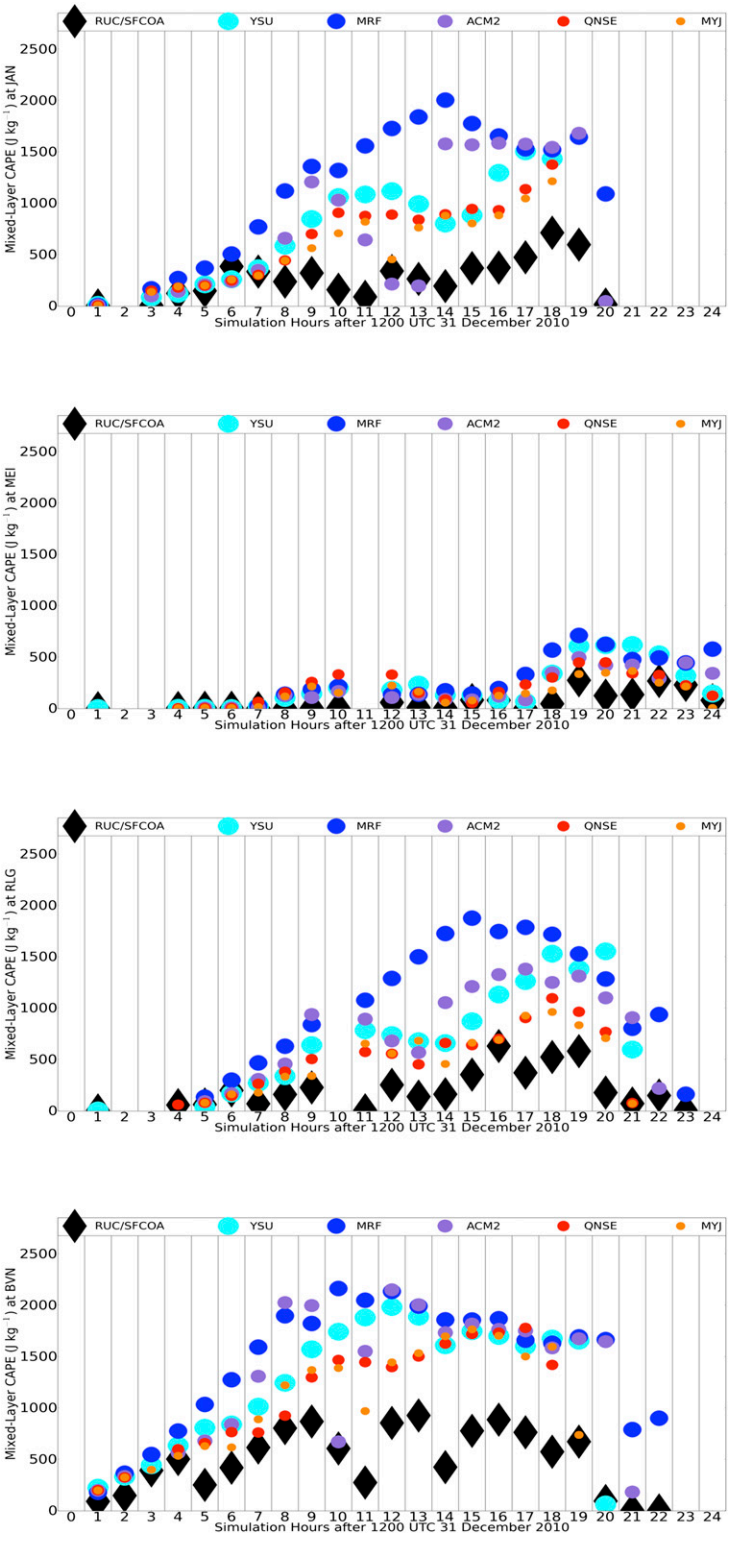

FIG. 11. As in Fig. 9, but for MLCAPE.

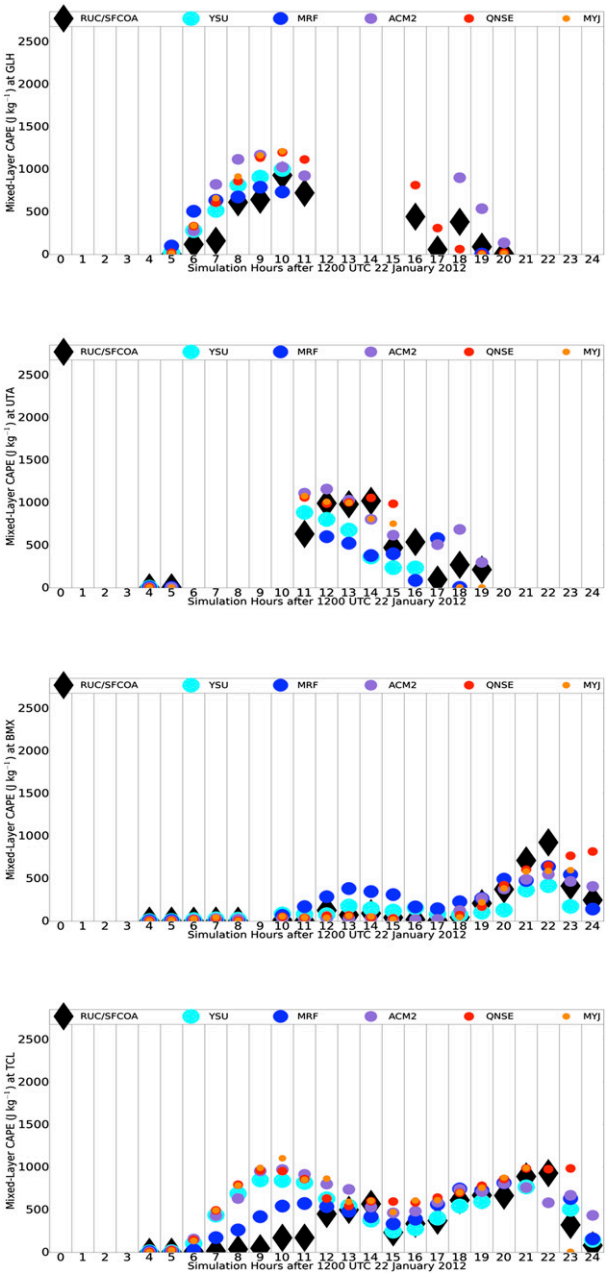

FIG. 12. As in Fig. 10, but for MLCAPE.

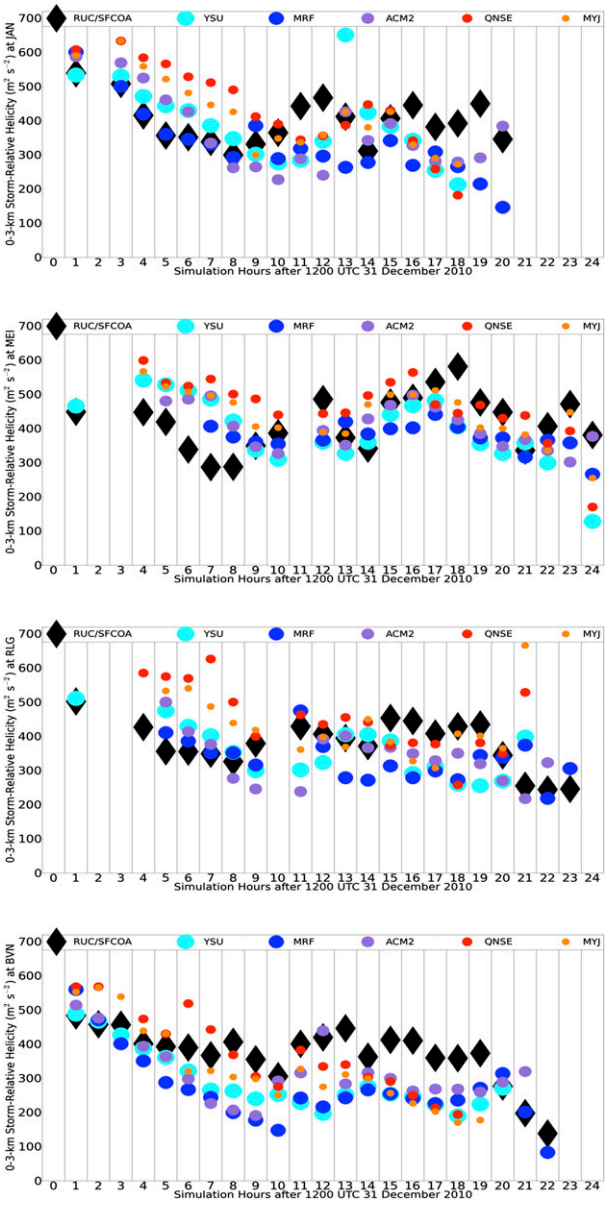

FIG. 13. As in Fig. 9, but for 0–3-km SRH.

than those studies that evaluate PBL schemes in a more ideal, slowly spatiotemporally evolving PBL in convective boundary layers. To select locations for comparison, it is important to represent the warm-sector environment upstream from convection that has not been contaminated by convection. At a given time, any one location may not have these conditions satisfied among all five WRF simulations and RUC–SFCOA. Therefore, the choice is made to focus on four sounding locations for each case owing to the intensive work needed to ensure that the near-storm environment sampled by the sounding had positive buoyancy and was not contaminated by convection in six different datasets and because relatively homogeneous conditions within the warm sector outside of convection would lead to redundancies in the analysis that four points resolves sufficiently. The 0–3-km temperature lapse rate (hereafter referred to as the 0–3-km lapse rate), 0–3-km storm-relative helicity[2]

[2] Storm motion is for a right-moving supercell using the Bunkers supercell motion technique in Bunkers et al. (2000).

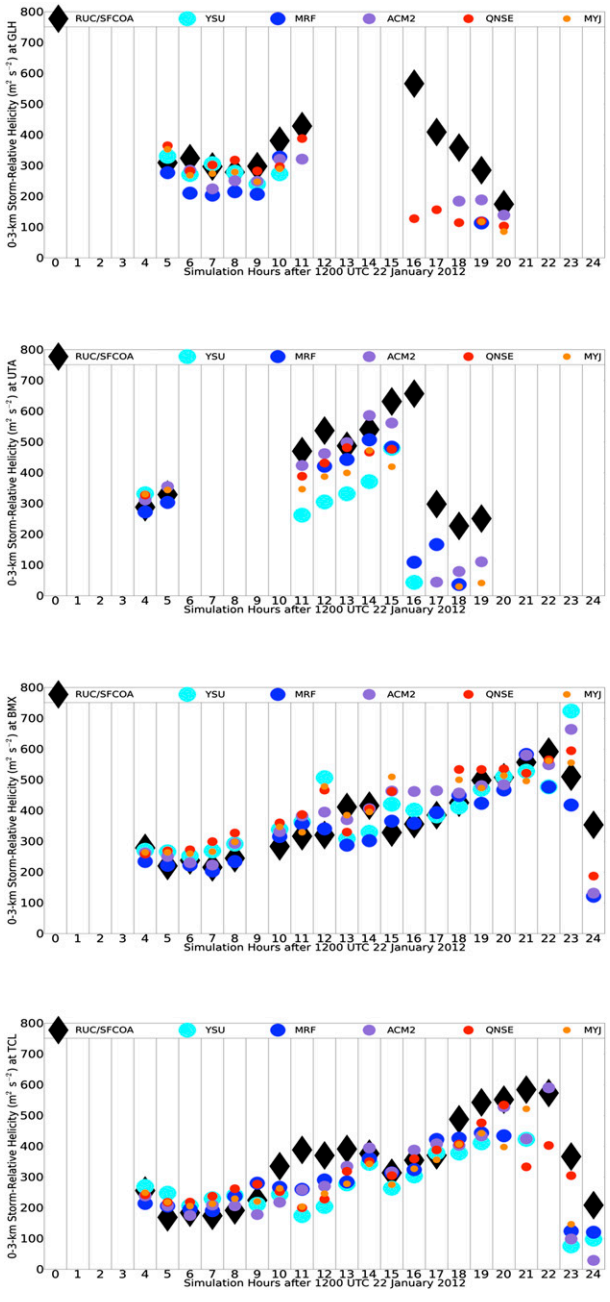

FIG. 14. As in Fig. 10, but for 0–3-km SRH.

(SRH), and mixed-layer CAPE derived from the mean conditions in the lowest 100 mb of the profile are computed from all soundings. These parameters provide clues in the diagnosis of the potential for severe weather (e.g., Thompson et al. 2003; Craven and Brooks 2004).

Statistical comparisons between simulated parameters and those derived from the RUC–SFCOA output are provided using a framework for error analysis. While this framework is often applied in economic forecast analysis (e.g., Theil 1961, 1966; Clements and Frenkel 1980; Pindyck and Rubinfeld 1981), its statistical applicability is broader among other fields (Trnka et al. 2006). Theil's inequality coefficient is defined as

$$U = \frac{\sqrt{\frac{1}{T}\sum_{t=1}^{T}(Y_t^s - Y_t^a)^2}}{\sqrt{\frac{1}{T}\sum_{t=1}^{T}(Y_t^s)^2} + \sqrt{\frac{1}{T}\sum_{t=1}^{T}(Y_t^a)^2}}. \quad (1)$$

Model forecasts and observations are indicated by Y_t^s and Y_t^a, respectively, while T represents the total sample size. The numerator represents the root-mean-square error (RMSE), and the quotient to determine U represents a normalized form of the RMSE. The benefit of considering a normalized form of the RMSE as opposed to strictly the RMSE is that the former permits standardization of error comparisons among parameters whose magnitudes vary greatly. Specifically, U can theoretically be as low as zero, representing a perfect forecast, with progressively higher values indicating poorer forecast quality. The bias proportion of U is defined as

$$U_m = \frac{(\overline{Y}^s - \overline{Y}^a)^2}{(1/T)\sum(Y_t^s - Y_t^a)^2}. \quad (2)$$

The quantity U_m represents that component of the error that is systematic (i.e., the bias). Values of this component roughly in excess of 0.1 or 0.2 indicate the presence of bias inherent in the forecast model. Since differences for thermodynamic and kinematic profiles among the WRF simulations do not become apparent until after the first hour of the simulation, comparisons between forecast and RUC–SFCOA output are not analyzed until at least 1 h into the simulation cycles.

b. Evaluation discussion

Schemes with nonlocal influences (i.e., YSU, MRF, and ACM2) provide noticeably steeper 0–3-km lapse rates than those provided by strictly local schemes (Figs. 9 and 10), and are commonly closer to those derived by RUC–SFCOA for the first severe weather event (Fig. 9). The WRF simulations typically yield overestimates of mixed-layer CAPE (MLCAPE) regardless of which scheme is used (Figs. 11 and 12), and the same nonlocal schemes that more accurately predict steeper lower-tropospheric lapse rates than local schemes in the first severe weather case yield more substantial overestimates of MLCAPE (Fig. 11). Between the two cases, WRF simulations and RUC–SFCOA mutually indicate around 200–500 $m^2 s^{-2}$ of

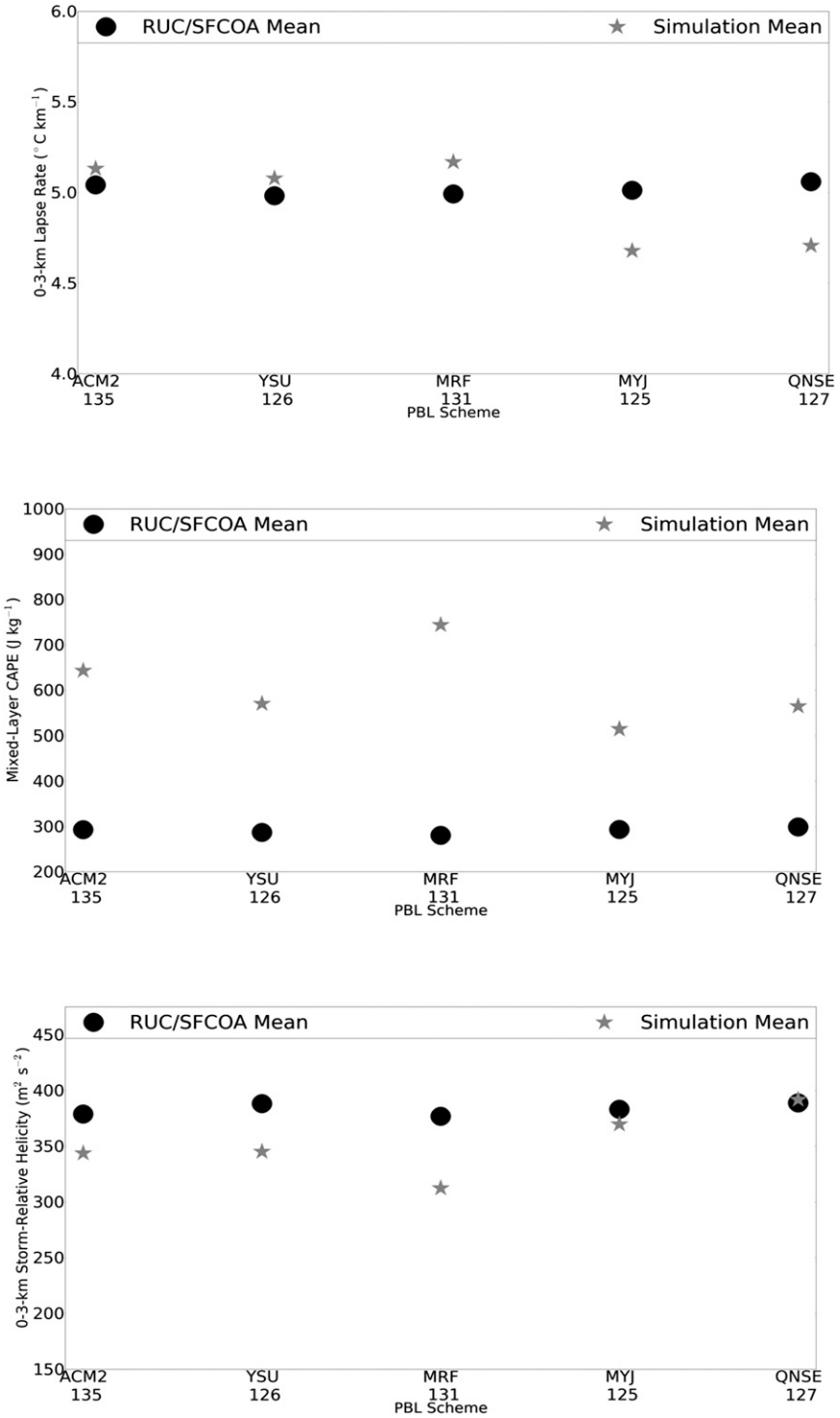

FIG. 15. Mean values of simulated and RUC–SFCOA-derived (top) 0–3-km lapse rate, (middle) MLCAPE, and (bottom) 0–3-km SRH among all PBL schemes, representing an aggregation among all sites identified in Fig. 5, with sample sizes listed along the abscissa. The black circles denote RUC–SFCOA values, whereas the gray stars denote simulation values. Note that minor differences in simulation means are explained by differences in analyzed times among corresponding PBLs (owing to variability in which soundings are convectively contaminated).

TABLE 3. Theil's inequality coefficient and the bias component for WRF simulations and RUC–SFCOA-derived 0–3-km lapse rate, MLCAPE, and 0–3-km SRH among all PBL schemes, representing an aggregation among all sites identified in Fig. 5.

Parameter	ACM2	YSU	MRF	MYJ	QNSE
0–3-km lapse rate	$U = 0.07$	$U = 0.07$	$U = 0.07$	$U = 0.08$	$U = 0.08$
	$U_m = 0.02$	$U_m = 0.02$	$U_m = 0.06$	$U_m = 0.17$	$U_m = 0.20$
MLCAPE	$U = 0.43$	$U = 0.42$	$U = 0.52$	$U = 0.34$	$U = 0.35$
	$U_m = 0.40$	$U_m = 0.32$	$U_m = 0.42$	$U_m = 0.35$	$U_m = 0.44$
0–3-km SRH	$U = 0.13$	$U = 0.16$	$U = 0.15$	$U = 0.14$	$U = 0.15$
	$U_m = 0.13$	$U_m = 0.12$	$U_m = 0.34$	$U_m = 0.02$	$U_m < 0.01$

0–3-km SRH (Figs. 13 and 14), with the nonlocal schemes often yielding relatively less SRH.

These overall differences are reflected in Fig. 15. Mean values of the low-level lapse rates are typically greater and more accurate for nonlocal schemes than local schemes. This is largely consistent with the results documented in many of the previously discussed studies that find stronger, deeper vertical mixing (which steepens lapse rates) as portrayed by the nonlocal schemes to more accurately represent the thermodynamic profile of a simulation compared to strictly local schemes. The vertical mixing tends environmental lapse rates toward dry adiabatic, and deeper mixing expands the vertical extent of these steeper environmental lapse rates. The strictly local schemes (i.e., MYJ and QNSE) exhibit greater bias than the nonlocal schemes for 0–3-km lapse rate (Table 3) and are associated with less steep 0–3-km lapse rates (Fig. 15). The MRF accentuates these characteristics, which is particularly evident with biases in its overestimation of the lower-tropospheric lapse rates (Table 3). This is entirely consistent with the tendency for this nonlocal scheme to represent too strong vertical mixing in strong-wind regimes, as suggested by Hong et al. (2006), yielding too much smoothing of the vertical wind profile and too small of SRH (Fig. 15), with SRH biases apparent in Table 3.

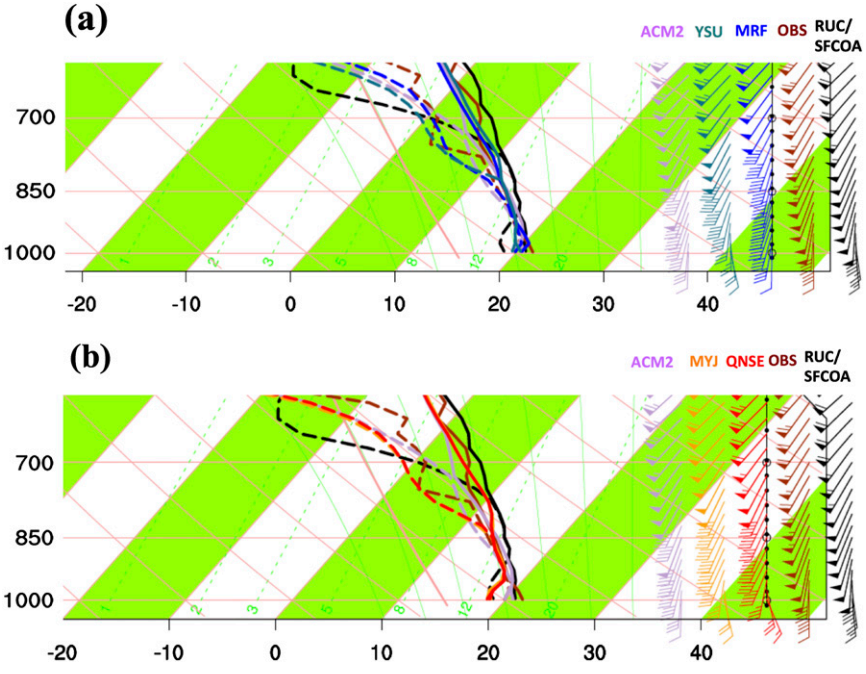

FIG. 16. Lower-tropospheric WRF sounding overlays from (a) nonlocal (YSU and MRF) and hybrid local and nonlocal (ACM2) schemes, and from (b) local (MYJ and QNSE) and hybrid local–nonlocal (ACM2) schemes, plotted around and below the 600-mb level at 0400 UTC 1 Jan 2011 for JAN, plotted beside soundings from the observed JAN sounding and corresponding RUC–SFCOA sounding. Sounding plotting format is similar to that illustrated in Fig. 4, with solid-line temperature profiles plotted to the right of the dashed-line dewpoint profile.

Otherwise, for 0–3-km SRH, neither error nor bias among the local or nonlocal schemes is particularly large.

Sensitivities in MLCAPE owing to the vertical integration of thermodynamic profiles through a deep layer of the troposphere provide a challenge in assessing the relative effect of modulations to the profiles by the PBL schemes, as such a parameter may be more influenced by secondary differences among the WRF simulations (e.g., convective evolution) to which a more simple lapse rate calculation would be more resistant. These concepts are associated with notably larger errors and biases in MLCAPE among all WRF simulations than the other aforementioned variables (Table 3).

Many of these statistical results are highlighted by the overlay of WRF soundings provided in Fig. 16, which also provides comparisons with the sounding output also plotted in Fig. 4 (observed sounding) and the corresponding RUC–SFCOA reconstructed sounding, all for the same time and location. The local schemes depict greater static stability in the near-surface layer, with greater directional shear, below the 850-mb level. On the other hand, the nonlocal schemes more accurately highlight warmer surface temperatures, less static stability, and a somewhat smoother vertical profile in the lower troposphere.

6. General discussion and conclusions

This study summarizes key characteristics that explain the differences among WRF PBL schemes along with advantages and disadvantages to using each scheme. Particular emphasis is placed on evaluating the performance of these schemes in modeling the lower-tropospheric thermodynamic and kinematic profile for southeastern U.S. cold season severe weather environments.

The primary difference between these schemes involves their representation of the vertical mixing process, in terms of the determination of which model layers influence atmospheric conditions at a given model level. Local schemes only permit nearby model layers to influence these conditions, precluding the direct inclusion of the effects that larger turbulent eddies yield in mixing atmospheric properties within much more vertically expansive depths of the lower troposphere. Nonlocal schemes consider the effect of these larger eddies on the dispersion of heat, moisture, and momentum throughout the depth of the PBL. As such, they are more likely to properly simulate the diurnally growing PBL owing to their inclusion of thermally driven turbulence associated with the diabatically heated surface layer. This is despite the potential for localized layers of relatively higher static stability to exist that may not have deleterious effects in building the PBL. Local schemes have more of a tendency to stunt the growth of the PBL owing to the presence of these statically stable layers when, in reality, the larger turbulent eddies can still mix through such localized layers.

As an example, through a test of five different PBL schemes for two southeastern U.S. cold season tornado events, WRF simulations that employ nonlocal parameterizations of the PBL produce 0–3-km lapse rates that are more accurate, less biased, and steeper than those that employ local-only schemes. This is consistent with the previously mentioned findings with respect to warm season, European PBLs, in which the nonlocal PBL scheme reduces biases in temperature forecasts in association with its ability to better simulate entrainment processes within the PBL, yielding a relatively deeper PBL during the daytime. As an extension to the vertical wind profile, these nonlocal schemes accurately indicate a large, low-level SRH environment, albeit slightly smaller than what local schemes indicate, suggesting that the deeper mixing did not unrealistically smooth the strong vertical wind shear in this environment. At the same time, both nonlocal and local schemes typically overestimate MLCAPE, though these overestimates are more prominent with nonlocal schemes.

There may not be a one-size-fits-all approach to the selection of such a ''best'' scheme. However, this study is intended to be a first step in gaining a better understanding of the relatively unexplored behavior of the PBL, and its representation in numerical weather models, for cold season severe weather environments. Future work is ongoing to expand and generalize the results of the case studies discussed here to include a wide array of cases, allowing a more substantial number of warm-sector points to be considered in cold season severe weather environments, among many other events.

Acknowledgments. Output displays use formats from the National Centers Advanced Weather Interactive Processing System Skew *T* Hodograph Analysis and Research Program (NSHARP; Hart et al. 1999). The authors thank Dr. Israel Jirak of the Storm Prediction Center, along with three anonymous reviewers, for their reviews of this paper and comments that have contributed to its improvement. The lead author thanks his father, Mr. Joel Cohen, an economist, for numerous discussions and insight regarding forecast evaluation. This work was originally inspired by the lead author's doctoral committee at the University of Oklahoma School of Meteorology for his Ph.D. General Examination. Committee members include Dr. Steven Cavallo, Dr. Harold Brooks, Dr. Frederick Carr, Dr. Kevin Kloesel, and Dr. John Greene.

APPENDIX

Procedure for Constructing RUC–SFCOA Soundings for Comparison with WRF Simulations

Gridded RUC output, at 20-km grid spacing, is provided by the NOAA National Model Archive and Distribution System (NOAA/NCDC 2014a,b). Basic thermodynamic and kinematic variables (i.e., temperature, relative humidity, and horizontal wind components) are extracted from the RUC vertical profile at 25-mb increments above the surface on an hourly basis through the 24-h simulation period. All calculations relating these variables are performed using the NCAR Command Language (NCL; NCAR 2014). Four profiles are selected for each hour, corresponding to the each of the sites identified in Fig. 5. The surface pressure and corresponding thermodynamic and kinematic values at each hour are provided from the SFCOA output (Bothwell et al. 2002). All data at higher pressures than this SFCOA baseline are deleted, effectively setting the SFCOA-related information as the base of the vertical profile (i.e., at the surface of the earth). All calculations related to integrated, composite parameters are performed on the subsequent merged soundings, following procedures applied in Coniglio et al. (2013), for example.

REFERENCES

Angevine, W. M., 2005: An integrated turbulence scheme for boundary layers with shallow cumulus applied to pollutant transport. *J. Appl. Meteor.,* **44,** 1436–1452, doi:10.1175/JAM2284.1.

——, H. Jiang, and T. Mauritsen, 2010: Performance of an eddy diffusivity–mass flux scheme for shallow cumulus boundary layers. *Mon. Wea. Rev.,* **138,** 2895–2912, doi:10.1175/2010MWR3142.1.

Ashley, W. S., 2007: Spatial and temporal analysis of tornado fatalities in the United States: 1880–2005. *Wea. Forecasting,* **22,** 1214–1228, doi:10.1175/2007WAF2007004.1.

Bothwell, P. D., J. A. Hart, and R. L. Thompson, 2002: An integrated three-dimensional objective analysis scheme in use at the Storm Prediction Center. Preprints, *21st Conf. on Severe Local Storms/19th Conf. on weather Analysis and Forecasting/15th Conf. on Numerical Weather Prediction,* San Antonio, TX, Amer. Meteor. Soc., JP3.1. [Available online at https://ams.confex.com/ams/pdfpapers/47482.pdf.]

Bougeault, P., and P. Lacarrère, 1989: Parameterization of orography-induced turbulence in a mesobeta-scale model. *Mon. Wea. Rev.,* **117,** 1872–1890, doi:10.1175/1520-0493(1989)117<1872:POOITI>2.0.CO;2.

Bretherton, C. S., and S. Park, 2009: A new moist turbulence parameterization in the Community Atmosphere Model. *J. Climate,* **22,** 3422–3448, doi:10.1175/2008JCLI2556.1.

Bright, D. R., and S. L. Mullen, 2002: The sensitivity of the numerical simulation of the southwest monsoon boundary layer to the choice of PBL turbulence parameterization in MM5. *Wea. Forecasting,* **17,** 99–114, doi:10.1175/1520-0434(2002)017<0099:TSOTNS>2.0.CO;2.

Brooks, H. E., 2009: Proximity soundings for Europe and the United States from reanalysis data. *Atmos. Res.,* **93,** 546–553, doi:10.1016/j.atmosres.2008.10.005.

Bunkers, M. J., B. A. Klimowski, J. W. Zeitler, R. L. Thompson, and M. L. Weisman, 2000: Predicting supercell motion using a new hodograph technique. *Wea. Forecasting,* **15,** 61–79, doi:10.1175/1520-0434(2000)015<0061:PSMUAN>2.0.CO;2.

Burk, S. D., and W. T. Thompson, 1989: A vertically nested regional numerical weather prediction model with second-order closure physics. *Mon. Wea. Rev.,* **117,** 2305–2324, doi:10.1175/1520-0493(1989)117<2305:AVNRNW>2.0.CO;2.

Ching, J., R. Rotunno, M. LeMone, A. Martilli, B. Kosovic, P. A. Jimenez, and J. Dudhia, 2014: Convectively induced secondary circulations in fine-grid mesoscale numerical weather prediction models. *Mon. Wea. Rev.,* **142,** 3284–3302, doi:10.1175/MWR-D-13-00318.1.

Clements, K. W., and J. A. Frenkel, 1980: Exchange rates, money and relative prices: The dollar–pound in the 1920s. *J. Int. Econ.,* **10,** 249–262, doi:10.1016/0022-1996(80)90057-4.

Coniglio, M. C., 2012: Verification of RUC 0–1-h forecasts and SPC mesoscale analyses using VORTEX2 soundings. *Wea. Forecasting,* **27,** 667–683, doi:10.1175/WAF-D-11-00096.1.

——, J. Correia, P. T. Marsh, and F. Kong, 2013: Verification of convection-allowing WRF Model forecasts of the planetary boundary layer using sounding observations. *Wea. Forecasting,* **28,** 842–862, doi:10.1175/WAF-D-12-00103.1.

Craven, J. P., and H. E. Brooks, 2004: Baseline climatology of sounding derived parameters associated with deep, moist convection. *Natl. Wea. Dig.,* **28,** 13–24.

Davies-Jones, R. P., D. Burgess, and M. Foster, 1990: Test of helicity as a forecasting parameter. Preprints, *16th Conf. on Severe Local Storms,* Kananaskis Park, AB, Canada, Amer. Meteor. Soc., 588–592.

Ek, M. B., K. E. Mitchell, Y. Lin, P. Grunmann, E. Rodgers, G. Gayno, and V. Koren, 2003: Implementation of the upgraded Noah land surface model in the NCEP operational mesoscale Eta model. *J. Geophys. Res.,* **108,** 8851, doi:10.1029/2002JD003296.

García-Díez, M., J. Fernández, L. Fita, and C. Yagüe, 2013: Seasonal dependence of WRF Model biases and sensitivity to PBL schemes over Europe. *Quart. J. Roy. Meteor. Soc.,* **139,** 501–514, doi:10.1002/qj.1976.

Gibbs, J. A., E. Fedorovich, and A. M. J. van Eijk, 2011: Evaluating Weather Research and Forecasting (WRF) Model predictions of turbulent flow parameters in a dry convective boundary layer. *J. Appl. Meteor. Climatol.,* **50,** 2429–2444, doi:10.1175/2011JAMC2661.1.

Grenier, H., and C. S. Bretherton, 2001: A moist PBL parameterization for large-scale models and its application to subtropical cloud-topped marine boundary layers. *Mon. Wea. Rev.,* **129,** 357–377, doi:10.1175/1520-0493(2001)129<0357:AMPPFL>2.0.CO;2.

Guyer, J. L., and A. R. Dean, 2010: Tornadoes within weak CAPE environments across the continental United States. Preprints, *25th Conf. on Severe Local Storms,* Denver, CO, Amer. Meteor. Soc., 1.5. [Available online at http://ams.confex.com/ams/pdfpapers/175725.pdf.]

——, D. A. Imy, A. Kis, and K. Venable, 2006: Cool season significant (F2–F5) tornadoes in the Gulf Coast states. Preprints, *23rd Conf. on Severe Local Storms,* St. Louis, MO, Amer. Meteor. Soc., 4.2. [Available online at https://ams.confex.com/ams/pdfpapers/115320.pdf.]

Hacker, J. P., 2010: Spatial and temporal scales of boundary layer wind predictability in response to small-amplitude land

surface uncertainty. *J. Atmos. Sci.,* **67,** 217–233, doi:10.1175/2009JAS3162.1.

Hart, J. A., J. Whistler, R. Lindsay, and M. Kay, 1999: NSHARP, version 3.10. Storm Prediction Center, National Centers for Environmental Prediction, Norman, OK, 33 pp.

Haylock, M. R., N. Hofstra, A. M. G. Klein Tank, E. J. Klok, P. D. Jones, and M. New, 2008: A European daily high-resolution gridded dataset of surface temperature and precipitation. *J. Geophys. Res.,* **113,** D20119, doi:10.1029/2008JD010201.

Holton, J. R., 2004: *Introduction to Dynamic Meteorology.* 4th ed. Elsevier, 535 pp.

Holtslag, A. A. M., and B. A. Boville, 1993: Local versus nonlocal boundary-layer diffusion in a global climate model. *J. Climate,* **6,** 1825–1842, doi:10.1175/1520-0442(1993)006<1825:LVNBLD>2.0.CO;2.

Hong, S.-Y., and H.-L. Pan, 1996: Nonlocal boundary layer vertical diffusion in a medium-range forecast model. *Mon. Wea. Rev.,* **124,** 2322–2339, doi:10.1175/1520-0493(1996)124<2322:NBLVDI>2.0.CO;2.

——, and J. O. J. Lim, 2006: The WRF single-moment 6-class microphysics scheme (WSM6). *J. Korean Meteor. Soc.,* **42,** 129–151.

——, S. Y. Noh, and J. Dudhia, 2006: A new vertical diffusion package with an explicit treatment of entrainment processes. *Mon. Wea. Rev.,* **134,** 2318–2341, doi:10.1175/MWR3199.1.

Hu, X.-M., J. W. Nielsen-Gammon, and F. Zhang, 2010: Evaluation of three planetary boundary layer schemes in the WRF Model. *J. Appl. Meteor. Climatol.,* **49,** 1831–1844, doi:10.1175/2010JAMC2432.1.

Huang, H.-Y., A. Hall, and J. Teixeira, 2013: Evaluation of the WRF PBL parameterizations for marine boundary layer clouds: Cumulus and stratocumulus. *Mon. Wea. Rev.,* **141,** 2265–2271, doi:10.1175/MWR-D-12-00292.1.

Iacono, M. J., J. S. Delamere, E. J. Mlawer, M. W. Shephard, S. A. Clough, and W. D. Collins, 2008: Radiative forcing by long-lived greenhouse gases: Calculations with the AER radiative transfer models. *J. Geophys. Res.,* **113,** D13103, doi:10.1029/2008JD009944.

Janjić, Z. I., 1990: The step-mountain coordinate: Physical package. *Mon. Wea. Rev.,* **118,** 1429–1443, doi:10.1175/1520-0493(1990)118<1429:TSMCPP>2.0.CO;2.

——, 1994: The step-mountain eta coordinate model: Further developments of the convection, viscous sublayer, and turbulence closure schemes. *Mon. Wea. Rev.,* **122,** 927–945, doi:10.1175/1520-0493(1994)122<0927:TSMECM>2.0.CO;2.

——, 1996: The surface layer in the NCEP Eta Model. Preprints, *11th Conf. on Numerical Weather Prediction,* Norfolk, VA, Amer. Meteor. Soc., 354–355.

Jankov, I., W. A. Gallus, M. Segal, B. Shaw, and S. E. Koch, 2005: The impact of different WRF Model physical parameterizations and their interactions on warm season MCS rainfall. *Wea. Forecasting,* **20,** 1048–1060, doi:10.1175/WAF888.1.

Johns, R. H., and C. A. Doswell III, 1992: Severe local storms forecasting. *Wea. Forecasting,* **7,** 588–612, doi:10.1175/1520-0434(1992)007<0588:SLSF>2.0.CO;2.

Kain, J. S., M. E. Baldwin, P. R. Janish, S. J. Weiss, M. P. Kay, and G. W. Carbin, 2003: Subjective verification of numerical models as a component of a broader interaction between research and operations. *Wea. Forecasting,* **18,** 847–860, doi:10.1175/1520-0434(2003)018<0847:SVONMA>2.0.CO;2.

——, S. J. Weiss, M. E. Baldwin, G. W. Carbin, D. A. Bright, J. J. Levit, and J. A. Hart, 2005: Evaluating high-resolution configurations of the WRF Model that are used to forecast severe convective weather: The 2005 SPC/NSSL Spring Program. Preprints, *21st Conf. on Weather Analysis and Forecasting/17th Conf. on Numerical Weather Prediction,* Washington, DC, Amer. Meteor. Soc., 2A.5. [Available online at http://ams.confex.com/ams/pdfpapers/94843.pdf.]

——, and Coauthors, 2013: A feasibility study for probabilistic convection initiation forecasts based on explicit numerical guidance. *Bull. Amer. Meteor. Soc.,* **94,** 1213–1225, doi:10.1175/BAMS-D-11-00264.1.

Kis, A. K., and J. M. Straka, 2010: Nocturnal tornado climatology. *Wea. Forecasting,* **25,** 545–561, doi:10.1175/2009WAF2222294.1.

Kosović, B., and J. A. Curry, 2000: A large eddy simulation study of a quasi-steady stably stratified atmospheric boundary layer. *J. Atmos. Sci.,* **57,** 1052–1068, doi:10.1175/1520-0469(2000)057<1052:ALESSO>2.0.CO;2.

Mass, C. F., D. Ovens, K. Westrick, and B. A. Colle, 2002: Does increasing horizontal resolution produce more skillful forecasts? *Bull. Amer. Meteor. Soc.,* **83,** 407–430, doi:10.1175/1520-0477(2002)083<0407:DIHRPM>2.3.CO;2.

Mauritsen, T., G. Svensson, S. S. Zilitinkevich, I. Esau, L. Enger, and B. Grisogono, 2007: A total turbulent energy closure model for neutrally and stably stratified atmospheric boundary layers. *J. Atmos. Sci.,* **64,** 4113–4126, doi:10.1175/2007JAS2294.1.

Mellor, G. L., and T. Yamada, 1974: A hierarchy of turbulence closure models for planetary boundary layers. *J. Atmos. Sci.,* **31,** 1791–1806, doi:10.1175/1520-0469(1974)031<1791:AHOTCM>2.0.CO;2.

——, and ——, 1982: Development of a turbulence closure model for geophysical fluid problems. *Rev. Geophys. Space Phys.,* **20,** 851–875, doi:10.1029/RG020i004p00851.

Monin, A. S., and A. M. Obukhov, 1954: Basic laws of turbulent mixing in the surface layer of the atmosphere (in Russian). *Tr. Geofiz. Inst., Akad. Nauk SSSR,* **24,** 1963–1967.

Nakanishi, M., and H. Niino, 2004: An improved Mellor–Yamada level-3 model with condensation physics: Its design and verification. *Bound.-Layer Meteor.,* **112,** 1–31, doi:10.1023/B:BOUN.0000020164.04146.98.

——, and ——, 2006: An improved Mellor–Yamada level-3 model: Its numerical stability and application to a regional prediction of advection fog. *Bound.-Layer Meteor.,* **119,** 397–407, doi:10.1007/s10546-005-9030-8.

——, and ——, 2009: Development of an improved turbulence closure model for the atmospheric boundary layer. *J. Meteor. Soc. Japan,* **87,** 895–912, doi:10.2151/jmsj.87.895.

NCAR, cited 2013: NCEP FNL operational model global tropospheric analyses, continuing from July 1999. Computational and Information Systems Laboratory, National Center for Atmospheric Research. [Available online at http://rda.ucar.edu/datasets/ds083.2/.]

——, cited 2014: NCAR Command Language. [Available online at http://www.ncl.ucar.edu/.]

Nielsen-Gammon, J. W., X.-M. Hu, F. Zhang, and J. E. Pleim, 2010: Evaluation of planetary boundary layer scheme sensitivities for the purpose of parameter estimation. *Mon. Wea. Rev.,* **138,** 3400–3417, doi:10.1175/2010MWR3292.1.

NOAA/NCDC, cited 2014a: Model Data Inventories. NOAA/National Operational Model Archive and Distribution System. [Available online at http://nomads.ncdc.noaa.gov/data.php?name=inventory.]

——, cited 2014b: RUC online archive. [Available online at http://nomads.ncdc.noaa.gov/data/ruc/.]

Pindyck, R. S., and D. L. Rubinfeld, 1981: *Econometric Models and Economic Forecasts.* 2nd ed. McGraw-Hill, 630 pp.

Pleim, J. E., 2007a: A combined local and nonlocal closure model for the atmospheric boundary layer. Part I: Model description and testing. *J. Appl. Meteor. Climatol.,* **46,** 1383–1395, doi:10.1175/JAM2539.1.

——, 2007b: A combined local and nonlocal closure model for the atmospheric boundary layer. Part II: Application and evaluation in a mesoscale meteorological model. *J. Appl. Meteor. Climatol.,* **46,** 1396–1409, doi:10.1175/JAM2534.1.

Rasmussen, E. N., and D. O. Blanchard, 1998: A baseline climatology of sounding-derived supercell and tornado forecast parameters. *Wea. Forecasting,* **13,** 1148–1164, doi:10.1175/1520-0434(1998)013<1148:ABCOSD>2.0.CO;2.

Schneider, J. M., and D. K. Lilly, 1999: An observational and numerical study of a sheared, convective boundary layer. Part I: Phoenix II observations, statistical description, and visualization. *J. Atmos. Sci.,* **56,** 3059–3078, doi:10.1175/1520-0469(1999)056<3059:AOANSO>2.0.CO;2.

Schneider, R. S., and A. R. Dean, 2008: A comprehensive 5-year severe storm environment climatology for the continental United States. Preprints, *24th Conf. on Severe Local Storms,* Savannah, GA, Amer. Meteor. Soc., 16A.4. [Available online at http://ams.confex.com/ams/pdfpapers/141748.pdf.]

Shin, H. H., and S.-Y. Hong, 2011: Intercomparison of planetary boundary-layer parameterizations in the WRF Model for a single day from CASES-99. *Bound.-Layer Meteor.,* **139,** 261–281, doi:10.1007/s10546-010-9583-z.

Skamarock, W. C., and Coauthors, 2008: A description of the Advanced Research WRF version 3. NCAR Tech. Note TN-475+STR, 113 pp. [Available online at http://www2.mmm.ucar.edu/wrf/users/docs/arw_v3.pdf.]

Stensrud, D. J., 2007: *Parameterization Schemes: Keys to Understanding Numerical Weather Prediction Models.* Cambridge University Press, 459 pp.

Storm Prediction Center, cited 2013a: SPC hourly mesoscale analysis. [Available online at http://www.spc.noaa.gov/exper/ma_archive/.]

——, cited 2013b: Storm Prediction Center National Severe Weather database browser: Online SeverePlot 3.0. [Available online at http://www.spc.noaa.gov/climo/online/sp3/plot.php.]

Stull, R. B., 1988: *An Introduction to Boundary Layer Meteorology.* Kluwer Academic, 666 pp.

——, 1991: Static stability—An update. *Bull. Amer. Meteor. Soc.,* **72,** 1521–1529, doi:10.1175/1520-0477(1991)072<1521:SSU>2.0.CO;2.

——, 1993: Review of non-local mixing in turbulent atmospheres: Transilient turbulence theory. *Bound.-Layer Meteor.,* **62,** 21–96, doi:10.1007/BF00705546.

Sukoriansky, S., B. Galperin, and V. Perov, 2005: Application of a new spectral theory of stably stratified turbulence to the atmospheric boundary layer over sea ice. *Bound.-Layer Meteor.,* **117,** 231–257, doi:10.1007/s10546-004-6848-4.

Theil, H., 1961: *Economic Forecasts and Policy.* 2nd Ed. North-Holland, 567 pp.

——, 1966: *Applied Economic Forecasting.* North-Holland, 474 pp.

Thompson, R. L., R. Edwards, J. A. Hart, K. L. Elmore, and P. Markowski, 2003: Close proximity soundings within supercell environments obtained from the Rapid Update Cycle. *Wea. Forecasting,* **18,** 1243–1261, doi:10.1175/1520-0434(2003)018<1243:CPSWSE>2.0.CO;2.

——, C. M. Mead, and R. Edwards, 2007: Effective storm-relative helicity and bulk shear in supercell thunderstorm environments. *Wea. Forecasting,* **22,** 102–115, doi:10.1175/WAF969.1.

Trnka, M., J. Eitzinger, G. Gruszczynski, K. Buchgraber, R. Resch, and A. Schaumberger, 2006: A simple statistical model for predicting herbage production from permanent grassland. *Grass Forage Sci.,* **61,** 253–271, doi:10.1111/j.1365-2494.2006.00530.x.

Troen, L., and L. Mahrt, 1986: A simple model of the atmospheric boundary layer: Sensitivity to surface evaporation. *Bound.-Layer Meteor.,* **37,** 129–148, doi:10.1007/BF00122760.

University Corporation for Atmospheric Research, cited 2014: Image archive meteorological case study collection kit. [Available online at http://www2.mmm.ucar.edu/imagearchive/.]

Vescio, M. D., and R. L. Thompson, 1998: Some meteorological conditions associated with isolated F3–F5 tornadoes in the cool season. Preprints, *19th Conf. on Severe Local Storms,* Minneapolis, MN, Amer. Meteor. Soc., 2–4.

Weiss, S. J., M. E. Pyle, Z. Janjić, D. R. Bright, and G. J. DiMego, 2008: The operational high resolution window WRF Model runs at NCEP: Advantages of multiple model runs for severe convective weather forecasting. Preprints, *24th Conf. on Severe Local Storms,* Savannah, GA, Amer. Meteor. Soc., P10.8. [Available online at http://ams.confex.com/ams/pdfpapers/142192.pdf.]

Wyngaard, J. C., and R. A. Brost, 1984: Top-down and bottom-up diffusion of a scalar in the convective boundary layer. *J. Atmos. Sci.,* **41,** 102–112, doi:10.1175/1520-0469(1984)041<0102:TDABUD>2.0.CO;2.

Xie, B., J. C.-H. Fung, A. Chan, and A. K.-H. Lau, 2012: Evaluation of nonlocal and local planetary boundary layer schemes in the WRF Model. *J. Geophys. Res.,* **117,** D12103, doi:10.1029/2011JD017080.